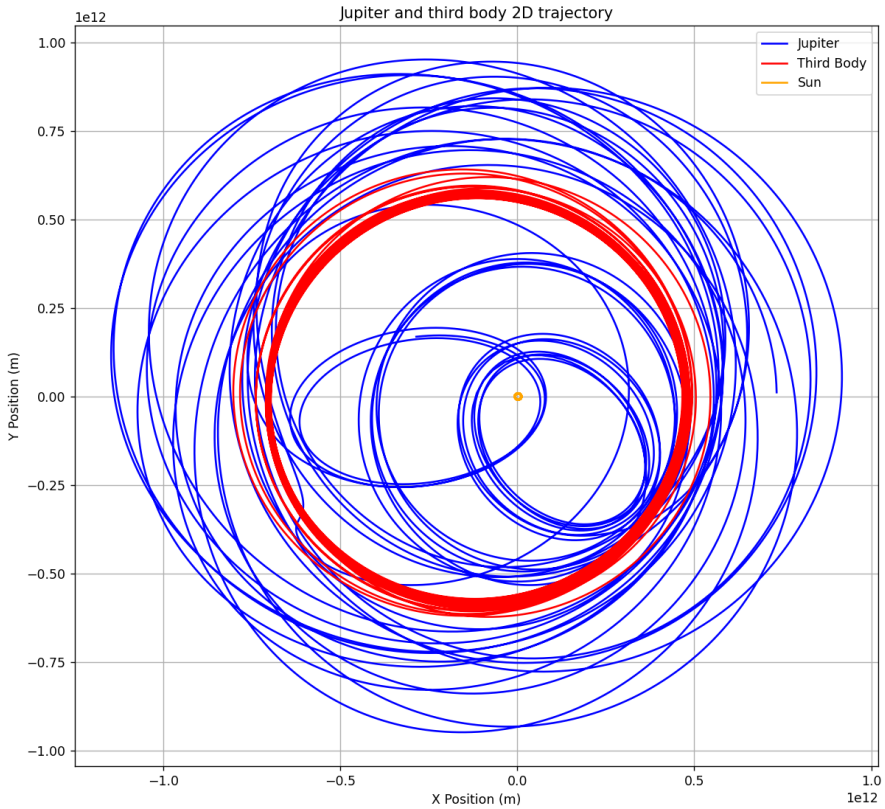

Simulation and analysis of planet impact parameters and their role on planetary configurations

Master's thesis in Physics

William Hillard

DEPARTMENT OF SPACE, EARTH AND ENVIRONMENT
CHALMERS UNIVERSITY OF TECHNOLOGY
Gothenburg, Sweden 2025
www.chalmers.se

Master's thesis 2025

Simulation and analysis of planet impact parameters and their role on planetary configurations

William Hillard

CHALMERS
UNIVERSITY OF TECHNOLOGY

Department of Space, Earth and Environment
Division of Astronomy and Plasma Physics
Chalmers University of Technology
Gothenburg, Sweden 2025

Simulation and analysis of planet impact parameters and their role on planetary configurations
William Hillard

Supervisor: Niloofar Khorshid, Department of Space, Earth and Environment
Assistant supervisor: Emil Knudstrup, Department of Space, Earth and Environment
Examiner: Carina Persson, Department of Space, Earth and Environment

Master's Thesis 2025
Department of Space, Earth and Environment
Division of Astronomy and Plasma Physics
Chalmers University of Technology
SE-412 96 Gothenburg
Telephone +46 31 772 1000

Cover: A figure showing the orbits of Jupiter and a third body around the Sun.

Typeset in LaTeX
Gothenburg, Sweden 2025

Simulation and analysis of planet impact parameters and their role on planet configurations

William Hillard
Department of Space, Earth and Environment
Chalmers University of Technology

Abstract

The aim of this thesis was to investigate the formation of hot Jupiters—gas giant exoplanets with short orbital periods—through the mechanism of high-eccentricity tidal migration (HETM). A numerical simulation framework was developed to model planetary systems using Newtonian gravitational dynamics in two dimensions. The simulations focused on three-body systems consisting of the Sun, Jupiter, and a fictive third planet. A wide range of initial parameters were varied for the third body, including its mass, semi-major axis, and eccentricity, in order to explore conditions that might lead to the formation of hot Jupiters. The results were analyzed using plots of orbital trajectories and evolution of eccentricities and semi-major axes.

The simulations revealed that strong interactions between the planets can excite Jupiter's orbital eccentricity under certain conditions, particularly when the third body is sufficiently massive and has an orbit close to Jupiter's. However, the simulations did not produce any hot Jupiters in stable orbits. Instead, many cases resulted in Jupiters with high eccentricities in dynamically unstable orbits, making it unclear whether these configurations could eventually evolve into hot Jupiters, and many simulations ended in either planetary ejections or collisions.

A comparison with existing literature revealed key differences, particularly the absence of non-Newtonian forces such as tidal dissipation and general relativity in this project's model. These effects are considered essential in the later stages of HETM. While the intended outcome was not achieved, the developed framework offers a strong foundation for future work involving more realistic physics and refined initial conditions.

Keywords: hot Jupiters, high-eccentricity tidal migration, planet migration, planetary system

Acknowledgements

First, I would like to thank my supervisor Niloofar Khorshid and my assistant supervisor Emil Knudstrup. Thank you both for all of your continuous support throughout this project, your knowledge and feedback has been greatly appreciated. I also want to thank my examiner Carina Persson for introducing and recommending this project to me, as well as overseeing it.

Lastly, a special thanks to my family for always supporting me through all my years at Chalmers, it means a great deal and I couldn't have done this without you.

William Hillard, Gothenburg, June 2025

List of Acronyms

Below is the list of acronyms that have been used throughout this thesis listed in alphabetical order:

HETM	High-Eccentricity Tidal Migration

Contents

List of Figures

1
Introduction

Planets are among the most fascinating and diverse outcomes of cosmic evolution, forming naturally in the aftermath of star birth and populating galaxies in vast numbers. However, understanding planets in all their sizes, compositions, and evolutionary stages presents a complex challenge for several reasons. One of the main challenges is that, unlike stars, planets do not emit light of their own but merely reflect the light from their host stars. This makes the detection of planets outside our solar system virtually impossible with the naked eye, requiring the development of indirect detection methods. Despite these observational challenges, technological advances in the late 20th century finally enabled the first successful detections of exoplanets.

1.1 Background

Prior to 1995 when the first exoplanet around a Sun-like star was detected [1], our perception of planets and how they form was shaped almost entirely by the architecture of our own solar system. As a result, many types of planets now known to be common were thought to be unlikely to exist. It was therefore a surprise when the first exoplanet discovered was a massive gas giant in a very close orbit around its star—a type now known as a *hot Jupiter*. According to preexisting models of planet formation, several issues made the existence of hot Jupiters difficult to explain. Yet, regardless of all the problems assumed for giant planets to exist near their host stars, these observations showed that they actually do exist. These discoveries highlighted the need for new or revised theories specifically aimed at explaining the formation and evolution of hot Jupiters.

One of the key reasons hot Jupiters are difficult to explain is that the inner regions of protoplanetary disks, where they are now found, are typically too hot and lack sufficient solid material to allow for the efficient formation of massive planetary cores [2]. Moreover, the intense radiation near the star makes it difficult for gas envelopes to accumulate and remain stable [3]. These physical limitations suggest that hot Jupiters likely formed farther from their host stars—beyond the so-called 'snow line'—and later migrated inward [4].

Since then, three main theories have been proposed to explain hot Jupiters existence: **in situ formation**, **disk migration**, and **high-eccentricity tidal migration**. The theory of **in situ formation** suggests that they form close to their

stars [5], in the same location where they were observed today. **Disk migration** on the other hand proposes that hot Jupiters form at much larger distances from their stars [6], and later on gradually migrate inward as it through interactions with the protoplanetary disk looses angular momentum. The theory of **high-eccentricity tidal migration** is similar to disk migration in that the planet forms at a larger distance and later closes in towards the star [3], but the method through which they migrate is different. This theory is divided into two steps, firstly the planet interacts gravitationally with a second body causing it to loose orbital angular momentum and the orbit to become highly elliptical. Secondly, tidal forces from the host star act on the planet, dissipating its orbital energy and circularizing its orbit over time, leaving it in a close in orbit around the star.

There are a few reasons as to why high-eccentricity tidal migration is a necessary theory. Notably, many hot Jupiters exhibit strong misalignments between their orbital planes and the spin axes of their host stars—misalignments that are hard to explain through smooth disk migration or in situ formation but arise naturally from high-eccentricity mechanisms [7]. Additionally, hot Jupiters are often found in systems without nearby planetary companions—especially small planetary companions, which is consistent with the disruptive nature of planet–planet scattering or secular interactions (explained in chapter 2.2.1.1)[7]. This project focuses on high-eccentricity tidal migration as a potential migration mechanism for hot Jupiters, using simulations to investigate the orbital dynamics involved.

1.2 Aim

The aim of this project is to utilize computer simulations to study how planetary configurations evolve over time, depending on the initial conditions of the system. More specifically the goal is to explore high-eccentricity tidal migration (HETM) as a method to form hot Jupiters. The simulations which will be done in Python using the Rebound software [8], will include our sun, Jupiter, and a third planetary body. The third body's; mass, initial eccentricity, and initial semi-major axis, will be varied in order to try to probe Jupiter into going through HETM. The results from the simulations will then be compared to some observed Jupiter-like planets, thus exploring a possible method of formation for these planets.

1.3 Limitations

Simulations to study the long term evolution of planetary systems with a certain minimum level of precision while varying multiple parameters requires a lot of time and computational power. Therefore in order to make this project feasible within the set amount of time and with the limited computational power I have available, some constraints need to be put in place.

Firstly I limit myself to systems with two planets, which simplifies calculations and shortens the runtime of the simulations. It also makes the system less chaotic in gen-

eral and decreases the amount of parameters to vary. This constraint does slightly limit the generality of the results but it still keeps it very realistic since there are many systems with no more than two planets.

Secondly I limit the amount of parameters to vary to three, namely; the mass, initial eccentricity, and initial semi-major axis of the third body. While it could be relevant to vary the same parameters for Jupiter, or include other parameters, for example inclination, this quickly becomes unfeasible to simulate. Hence the parameters chosen to vary are the ones I thought have the biggest impact on the planetary configuration.

1.4 Outline

Chapter 2 introduces the relevant theory of hot Jupiters and their formation, and orbital mechanics. In Chapter 3, the methods used throughout this project to obtain the results are presented. Chapter 4 then displays all of the most relevant results. In Chapter 5, important findings from the project are discussed, and the conclusions are summarized in Chapter 6.

2

Theory

This section provides the theory necessary for this project, namely; hot Jupiters, an overview of general planet formation, planet formation specifically for hot Jupiters, and orbital mechanics.

2.1 Hot Jupiters

Hot Jupiters, as their name suggests, are Jupiter-like planets but much hotter. They are characterized by their large masses and very short orbital periods. Typically, hot Jupiters are defined as gas giants with masses comparable to or greater than that of Jupiter (M_{Jup}) and orbital periods of less than 10 days [3]. This places them extremely close to their host stars—often within 0.1 AU—resulting in significantly higher surface temperatures than gas giants located farther out in planetary systems.

Despite their similarity in mass to Jupiter, hot Jupiters differ considerably in physical and atmospheric properties because of their proximity to their stars. Many have equilibrium temperatures ranging from 1000 to over 2500 K [9]. Due to the strong tidal forces from their host stars, hot Jupiters are generally expected to be tidally locked, meaning they always present the same hemisphere toward the star [10]. This creates permanent day and night sides, leading to large temperature gradients and vigorous atmospheric circulation.

Since the discovery of the first planet, 51 Pegasi b, hundreds of hot Jupiters have been found [11], largely due to their detectability via both the radial velocity and transit method, which currently are the two most successful methods of detection of exoplanets. Their short periods increase the likelihood of repeated observations, while their large radii enhance the depth of transit signals. As a result, they were among the first and most commonly detected types of exoplanets, particularly in early surveys such as those by the Kepler and WASP missions [12][13].

Although hot Jupiters represent only a fraction of all known exoplanets today [11], they have played a central role in shaping the field of exoplanetary science. Their unexpected existence forced a major re-evaluation of planet formation theories and led to new questions about orbital migration, dynamical interactions, and tidal evolution. Beyond their historical significance, hot Jupiters continue to be scientifically valuable today due to the challenges they pose to existing formation models and the wealth of data they provide. Their large sizes and short periods make them prime

targets for atmospheric characterization via transmission and emission spectroscopy.

In summary, hot Jupiters naturally tests theories of planetary migration and dynamical interactions. However, despite the progress made, many questions remain—particularly regarding how such massive planets ended up so close to their stars. To address these questions, we must first explore the broader processes involved in planet formation and the different pathways by which planets can evolve over time.

2.2 Planet formation

Planet formation is a natural consequence of star formation, taking place within the protoplanetary disks that surround young stars. These disks, which typically persist for a few million years, serve as the environments where microscopic solid particles grow into full-fledged planets [14]. Understanding how this process unfolds is essential for explaining the wide variety of planetary systems observed today.

A typical protoplanetary disk consists primarily of hydrogen and helium gas, with a small fraction of heavier elements in the form of dust grains. The disk has a temperature gradient: the inner regions are hot, while the outer regions are colder. A key feature is the snow line, the distance from the star beyond which the temperature is low enough for volatile compounds like water to condense into their solid phase. This transition significantly increases the surface density of solids, making the formation of massive planetary cores more efficient in these outer regions [2].

The process begins with the growth of dust grains through coagulation into millimeter-sized pebbles, which eventually form kilometer-scale planetesimals via mechanisms like streaming instability [15]. Streaming instability is a collective effect where the relative motion between solid particles and gas in the protoplanetary disk causes the dust to concentrate and collapse gravitationally into larger bodies [15]. These planetesimals undergo mutual collisions and gravitational focusing, leading to the formation of planetary embryos—Moon- to Mars-sized bodies that can further accrete solids and gas.

Two main models have been proposed for the formation of gas giants. One of those models is the core accretion model, in which a solid core of roughly 10 Earth masses forms first and then accretes a gaseous envelope from the surrounding disk [4]. This process is relatively slow and typically requires the core to form beyond the snow line, where solid materials are more abundant. An alternative is the disk instability model, where a massive and cool protoplanetary disk becomes gravitationally unstable and fragments directly into self-gravitating clumps that collapse into gas giants [16]. This mechanism is much faster but may require more extreme disk conditions than are typically observed.

Once formed, planets are not expected to remain in their original orbits. Migration—driven by gravitational interactions with the disk (Type I or II migration) or

with other planets—can significantly reshape planetary systems [6]. In particular, gas giants can migrate inward from their formation sites beyond the snow line, potentially ending up on orbits much closer to their stars than where they originally form.

While general models of planet formation can account for many observed planetary architectures, they face a big challenge when trying to explain planets like hot Jupiters. This has led to the development of specific formation and migration theories tailored to explain the existence of these systems, which are the focus of the following section.

2.2.1 Migration of hot Jupiters

So how do hot Jupiters differ from the general formation and migration theory of gas giants? In standard models, gas giants are believed to form beyond the snow line, where low temperatures allow volatile compounds to condense into solids, facilitating the growth of massive planetary cores and the accretion of gaseous envelopes [4][2]. However, hot Jupiters are found extremely close to their host stars, where conditions are too hot and the solid material too scarce to efficiently form massive cores. Moreover, the high temperatures and strong stellar radiation in these inner regions make gas retention difficult and significantly hinder the runaway gas accretion process needed to form a gas giant.

Another critical constraint comes from disk lifetimes. Protoplanetary disks typically dissipate within 1–10 million years [14], meaning that any gas giant formation and subsequent orbital evolution must occur within this relatively short window. The proximity of hot Jupiters to their host stars, combined with these formation barriers and timing constraints, suggests that they likely did not form in their current locations, but rather originated farther out and later migrated inward.

To explain how hot Jupiters end up in close-in orbits, the three main migration pathways that have been proposed are: in situ formation, disk migration, and high-eccentricity tidal migration. Each of these mechanisms attempts to account for their observed orbital characteristics, though they vary in the processes involved and the timescales over which they operate.

The first proposed mechanism is in situ formation, which suggests that hot Jupiters formed near their present locations, very close to the star [17]. This scenario requires an unusually dense and metal-rich inner disk to allow the rapid accumulation of solid material and subsequent gas accretion. While this mechanism cannot be ruled out entirely, it faces significant theoretical challenges due to the difficulty of forming large planetary cores and sustaining gas accretion in such extreme environments.

A second widely discussed mechanism is disk-driven migration, in which hot Jupiters form at several astronomical units from the star and then migrate inward through gravitational interactions with the protoplanetary disk [18]. This process can naturally bring a planet inward over a few hundred thousand years while the disk is still

present. Disk migration is supported by simulations and explains the low eccentricities and aligned spin-orbit angles observed in many systems. However, it struggles to account for systems where the planet's orbit is significantly misaligned with the stellar equator, or retrograde—cases that suggest a more chaotic dynamical history. An alternative to these smooth processes is high-eccentricity tidal migration. This mechanism offers another compelling explanation for the existence of hot Jupiters and will be explored in more detail in the next section.

2.2.1.1 High-eccentricity tidal migration

High-eccentricity tidal migration is one of the leading mechanisms proposed to explain the presence of hot Jupiters—gas giants on extremely close-in orbits around their host stars. Unlike disk-driven migration, which occurs during the presence of the protoplanetary disk, HETM typically begins *after* disk dispersal and involves a two-step process. First, a Jupiter-like planet's orbit is excited to a high eccentricity ($e \gtrsim 0.9$) via gravitational interactions with a third body. Then, tidal forces raised during close periastron passages gradually dissipate energy, leading to inward migration and orbital circularization over timescales of millions to billions of years [3]. There are several mechanisms capable of driving a planet's orbital eccentricity to the extreme values needed for HETM to occur.

One such method of inducing a high eccentricity is planet–planet scattering, which is where strong gravitational interactions between giant planets, result in close encounters. Planet-planet scattering is possible in systems with 2 or more planets that are massive enough and close enough to each other, such that there is significant gravitational interaction between them. The maximum eccentricity achievable through scattering is limited by orbital energy conservation of the system and the escape velocity from the planetary surface. Dawson & Johnson (2018) approximate the limit for the eccentricity, e, of a scattered planet as:

$$e_{\text{scatter}} \lesssim 0.2 \left(\frac{M_p}{0.5 M_{\text{Jup}}}\right)^{1/2} \left(\frac{2R_{\text{Jup}}}{R_p}\right)^{1/2} \left(\frac{P}{3\,\text{days}}\right)^{1/3}, \tag{2.1}$$

where M_p and R_p are the mass and radius of the scattered planet, and P is its orbital period [3]. While scattering can produce high eccentricities quickly (on timescales of 10^3–10^6 years), it tends to be very chaotic and may lead to the loss of one or more planets in the form of ejections from the system or collisions with the star or another planet.

Another, more gradual mechanism to produce high eccentricities is secular interactions. In this scenario the planets exchange angular momentum over long timescales without close encounters [19]. They do not exchange orbital energy though, which leads the semi-major axis of the planets to remain the same. A major difference compared to planet-planet scattering is that there is a larger separation between the planets for secular interactions, reducing the planets gravitational effects on each other and making it less chaotic [3]. In systems with three or more planets, overlapping secular resonances can result in chaotic evolution known as *secular chaos*.

This can cause a planet's eccentricity to undergo a random walk, reaching noticeably high values over very long timescales [19]. Importantly, secular interactions allow eccentricity excitation to occur well after the disk has dissipated, aligning well with HETM timescales.

In systems with a distant, inclined companion (planetary or stellar), gravitational perturbations can induce Kozai–Lidov oscillations, leading to periodic exchanges between inclination and eccentricity [20]. Though this mechanism is less emphasized in this work, it remains a viable pathway in certain architectures.

Once a planet's eccentricity has been sufficiently excited by one of the previously discussed methods, its periastron (the planet's closest point to the star), defined as $q = a(1 - e)$, where a is the planet's semi-major axis, can approach distances where tidal forces from the star become significant [21]. At each close passage, the planets orbital energy is dissipated (and to a much lesser extent, the star), shrinking both the semi-major axis and the eccentricity, while the periastron, q, remains approximately constant [21]. This process conserves angular momentum while reducing orbital energy. The final circular orbit obeys the relation:

$$a_{\text{final}} = a(1 - e^2), \tag{2.2}$$

where a is the semi-major axis and e the orbital eccentricity before circularization [22]. For example, a planet starting tidal dissipation at $a = 2$ AU with $e = 0.99$ will circularize to a final orbit at $a \approx 0.04$ AU, which is characteristic of hot Jupiters.

The timescale and efficiency of tidal circularization is governed by multiple factors. Firstly it has a very strong dependence on a_{final} in such a way that the larger a_{final} is, the longer time it takes for tidal circularization to complete [3]. Another factor is the planet's tidal quality factor Q_p, which quantifies how effectively tidal energy is dissipated inside the planet. The timescale for circularization, which can be estimated from the equilibrium tide model [23], scales with Q_p as [24]:

$$\tau_{\text{circ}} \propto Q_p \left(\frac{a}{R_p} \right)^5, \tag{2.3}$$

Typical values for Q_p in gas giants range from 10^5 to 10^7, though this remains a major source of uncertainty in modeling tidal evolution [22].

As tidal dissipation circularizes the orbit and shrinks the semi-major axis, the influence of the original perturber (which excited the eccentricity) diminishes [3]. This *decoupling* occurs once other precession sources dominate the dynamics over the perturber. From this point onward, the evolution proceeds mostly under the effect of tides alone. During this phase, a planet undergoing HETM follows a trajectory of nearly constant orbital angular momentum, since angular momentum is largely conserved throughout tidal dissipation [22]. These trajectories defined by equation 2.2 can be used for a planet undergoing HETM to estimate how its previous orbit looked, and to project how it will evolve.

HETM provides a compelling explanation for several observed characteristics of hot Jupiters, including high obliquities or spin-orbit misalignments, isolated orbital architectures with few close planetary companions, and populations of moderately eccentric ($e \sim 0.2$–0.6) hot Jupiters consistent with ongoing tidal circularization [3]. However, a key challenge for the HETM scenario is the relative scarcity of observed super-eccentric proto-hot Jupiters—planets with $e > 0.9$ in the process of migrating. Dong et al. suggest this may be due to the short observational timescales spent at extreme eccentricities and possible observational biases against detecting such systems [22].

2.3 Orbital mechanics

To fully define an orbit there are six orbital elements you need. These are, semi-major axis a, eccentricity e, inclination i, right ascension of the ascending node Ω, argument of perigee ω, and mean anomaly M (or true anomaly θ) [25]. However, if you only consider orbits in two dimensions (which is true for this project), then you only need a, e, and M (or θ) for the orbit to be fully defined. Using these parameters, we can calculate every other magnitude that is necessary for propagating the motion of the body and analyzing the system.

To start, we begin by solving *Kepler's equation*, which relates the mean anomaly M to the eccentric anomaly E [26]:

$$M = E - e \sin E. \tag{2.4}$$

This equation is solved numerically to find E, given values of M and e.
Once E is known, we can calculate the orbital radius r, which gives the distance between the orbiting body and the central mass at a given point in the orbit [26]:

$$r = a(1 - e \cos E). \tag{2.5}$$

Next, the true anomaly θ, which gives the angle between the periapsis and the current position of the body, is computed from E using [26]

$$\theta = 2 \arctan \left(\sqrt{\frac{1+e}{1-e}} \tan \frac{E}{2} \right). \tag{2.6}$$

To be able to calculate following quantities like velocity, we first need to compute the specific angular momentum h of the orbit, which can be done by [25]

$$h = \sqrt{\mu a (1 - e^2)}, \tag{2.7}$$

where $\mu = G(M + m)$ is the standard gravitational parameter, and is usually approximated as GM when $m \ll M$.
Using h, we calculate the radial and tangential velocity components at any point along the orbit [25]:

$$v_r = \frac{\mu}{h} e \sin \theta, \quad v_\theta = \frac{\mu}{h}(1 + e \cos \theta). \tag{2.8}$$

These components can then be used to compute the position and velocity vectors in Cartesian coordinates. In two dimensions, the position vector is [27]

$$\begin{bmatrix} x \\ y \end{bmatrix} = r \begin{bmatrix} \cos\theta \\ \sin\theta \end{bmatrix}, \tag{2.9}$$

and the velocity vector in Cartesian coordinates is constructed using the radial and tangential components and their respective directions [27]:

$$\begin{bmatrix} v_x \\ v_y \end{bmatrix} = v_r \begin{bmatrix} \cos\theta \\ \sin\theta \end{bmatrix} + v_\theta \begin{bmatrix} -\sin\theta \\ \cos\theta \end{bmatrix}.$$

Given the velocity and position, we can compute the specific orbital energy for each body as [28]

$$\epsilon = \frac{1}{2}||v||^2 - \frac{\mu}{|r|}. \tag{2.10}$$

It can also be used to re-calculate the specific angular momentum [28]

$$\vec{h} = |\vec{r} \times \vec{v}|, \tag{2.11}$$

and the eccentricity [25]

$$e = \sqrt{1 + \frac{2\epsilon h^2}{\mu^2}}. \tag{2.12}$$

In simulations involving multiple interacting bodies, accelerations due to the gravitational forces from all other masses must be computed. For a given body i, this is done using [27]:

$$\vec{a}_i = \sum_{j \neq i} G m_j \frac{\vec{r}_j - \vec{r}_i}{|\vec{r}_j - \vec{r}_i|^3}. \tag{2.13}$$

For a multi-body system such as the one considered in this project with a Sun, Jupiter, and a third planet, you can also track the total energy and angular momentum of the system. These are useful to verify the accuracy of the numerical integration and the conservation laws.

The total mechanical energy of the system includes the kinetic energy of Jupiter and the third body, as well as the gravitational potential energy from their interactions with the Sun and with each other [25]:

$$E_{\text{total}} = \frac{1}{2} M_{\text{J}} \|\vec{v}_{\text{J}}\|^2 + \frac{1}{2} M_{\text{t}} \|\vec{v}_{\text{t}}\|^2 - G M_{\odot} \left(\frac{M_{\text{J}}}{\|\vec{r}_{\text{J}}\|} + \frac{M_{\text{t}}}{\|\vec{r}_{\text{t}}\|} \right) - \frac{G M_{\text{J}} M_{\text{t}}}{\|\vec{r}_{\text{J}} - \vec{r}_{\text{t}}\|}. \tag{2.14}$$

Similarly, the total angular momentum is given by [27]:

$$\vec{L}_{\text{total}} = |M_{\text{J}}(\vec{r}_{\text{J}} \times \vec{v}_{\text{J}}) + M_{\text{t}}(\vec{r}_{\text{t}} \times \vec{v}_{\text{t}})|. \tag{2.15}$$

In orbital mechanics, both energy and angular momentum are key conserved quantities, but their conservation depends on the assumptions and complexity of the system [25]. In a two-body problem with no external perturbations, both the *specific orbital energy* and *specific angular momentum* of each body are conserved [28].

This means that for a single planet orbiting a star, the shape and size of the orbit remain constant over time.

However, in a multi-body system such as the one studied in this project, these quantities are no longer strictly conserved for individual planets. Gravitational interactions between the planets can lead to exchanges of energy and angular momentum. In such cases, while the *specific* quantities of each planet can vary significantly—especially during close encounters—the *total mechanical energy* and *total angular momentum* of the full system is still conserved, assuming the system is isolated and no external forces act on it [25].

In dynamically stable configurations, changes in specific energy and angular momentum are gradual and predictable. However, in chaotic scenarios—such as when close encounters occur between planets—strong gravitational interactions can cause rapid changes in orbital parameters, and the total energy and angular momentum must be monitored to ensure that they are conserved. In this project, tracking the total energy and total angular momentum serves as an important diagnostic to assess whether the simulation remains physically accurate, even in the presence of such chaotic interactions.

3
Methods

This chapter describes how this project was carried out. It specifically provides explanations of how the simulations were set up and carried out and all the different types of figures that were produced. There is also a short section describing the comparison that was done between my simulations, real observed planets, and other scientific papers which conducted similar projects to this.

3.1 Computer simulations

All of the simulations and data analysis in this project was done in Python. To begin with, I built my own code from scratch to perform the simulations. However, later on I switched and started to utilize the already built Rebound software, and continued to do so for the remainder of the project.

3.1.1 My code

My code was developed to closely follow the structure outlined in the orbital mechanics section of the theory (Section 2.3). Before I could begin running long-term simulations with varying parameters, I first needed to implement a single simulation with fixed initial conditions to verify that the code was functioning correctly. I started by defining the relevant constants for the system: the gravitational constant G, and the masses m of the Sun, Jupiter, and the third planetary body. In addition, I specified the six classical orbital elements — a, e, i, ω, Ω, and θ — for both Jupiter and the third body. The parameters that remained constant throughout all of the project was the mass of the Sun ($M_{Sun} = 1.989 \times 10^{30} kg$) and Jupiter ($M_{Jup} = 1.898 \times 10^{27} kg$), the initial semi-major axis of Jupiter ($a = 5.20283$ AU), and the initial eccentricity of Jupiter ($e = 0.0484$). Initially, the third body's orbital parameters were set equal to those of Earth to provide a baseline test case for validating the simulation's correctness. This configuration was intended as a starting point and would later be altered in subsequent simulations. The Sun, due to its significantly larger mass compared to the planets, was assumed to remain fixed at the origin.

After defining all the input parameters, the next step was to convert the orbital elements into Cartesian coordinates in order to facilitate the numerical computations. Once all relevant vectors were expressed in Cartesian form, I implemented the necessary functions for calculating gravitational acceleration between the bodies, the

specific orbital energy and angular momentum of each planet, the total energy and angular momentum of the system, and the orbital eccentricity. These calculations were based on equations 2.10 through 2.15.

With all core quantities in place, I proceeded to construct the simulation itself. This consisted of a loop over discrete time steps, in which all dynamical quantities were updated in an Euler-like fashion. To store the evolution of the system for later analysis, I initialized empty lists for each variable of interest. The time step was chosen to be 86,400 seconds (equivalent to one Earth day), and the number of iterations was set to 4,380, so that the total simulated duration would correspond approximately to one full orbital period of Jupiter around the Sun. Within the loop, the gravitational accelerations, velocities, and positions of both planets were calculated and updated at each step. All other relevant quantities — such as energy, angular momentum, and eccentricity — were also computed and saved during each iteration.

After conducting initial tests and reviewing relevant literature, I identified a potential improvement to the simulation's accuracy: using a more stable integration scheme. I decided to replace the simple Euler-like method with the leapfrog integrator, an algorithm well-suited for gravitational systems. Leapfrog works by staggering the updates of position and velocity in time, effectively allowing them to "leap over" each other — hence the name [29].

The algorithm proceeds as follows: first, the velocity is updated by half a time step, then the position is updated using the intermediate velocity, and finally the velocity is updated again by another half step using the new acceleration. This process is described by the equations:

$$\vec{v}\left(t+\frac{\Delta t}{2}\right) = \vec{v}(t) + \frac{\Delta t}{2}\vec{a}(t), \tag{3.1}$$

$$\vec{r}(t+\Delta t) = \vec{r}(t) + \Delta t, \vec{v}\left(t+\frac{\Delta t}{2}\right), \tag{3.2}$$

$$\vec{v}(t+\Delta t) = \vec{v}\left(t+\frac{\Delta t}{2}\right) + \frac{\Delta t}{2}\vec{a}(t+\Delta t). \tag{3.3}$$

This integration method is both time-reversible and symplectic, meaning that it approximately preserves energy and angular momentum even over long durations. These properties make leapfrog particularly effective and reliable for simulating planetary dynamics [29].

3.1.1.1 Output

At this point, the simulation was complete and the relevant data had been saved. The next step was simply to select which figures to generate and analyze. The first and primary figure plotted was the orbital paths in two dimensions — specifically, the x- and y-positions of Jupiter and the third body over time. This provides a general overview of how the planets orbit the Sun, and by using Earth as the third

body, it becomes easy to assess whether the simulation produces reasonable and expected behavior. However, to more rigorously evaluate the correctness of the results, additional quantities must be examined.

Since the total energy and total angular momentum of the system should be conserved, both were plotted over time to verify this expected behavior. For the case in which the third body is Earth — a configuration known to be highly stable — the specific orbital energy and specific angular momentum of each planet should remain nearly constant, exhibiting only minimal fluctuations over time. These quantities were therefore also plotted. Finally, the eccentricity of both planets was plotted, with the expectation that it too would remain effectively constant throughout the simulation.

With these results obtained, the analysis of the figures could begin. Once this baseline case was completed, the initial conditions of the third body were systematically varied to explore a wide range of scenarios, focusing in particular on trying to induce large eccentricities of Jupiter. At this stage, a natural question arose: how can I be confident that my simulation code is as accurate as possible, and is there any way to improve it? While creating and analyzing the figures is a good test of general correctness, it remains a numerical simulation — and therefore subject to potential sources of error. To assess the accuracy and reliability of the implementation, the same simulations and corresponding figures were produced using the *Rebound* software, allowing for direct comparison and validation of the custom code.

3.1.2 Rebound

Rebound is a well-established open-source N-body integrator, meaning that it has the ability to create N-body simulations and integrate the motion of the bodies under the influence of gravity [8]. It was created mainly to accurately solve problems within astrophysics, and more specifically N-body collision dynamics [30].

3.1.2.1 Integrators

The Rebound software has a wide range of integrators implemented that one can choose from. To begin with I used the normal leapfrog integrator which works in the same way as in my own code. However after some research I realized that this probably was not the optimal choice. The two other integrators that I used instead throughout the project were **IAS15** and **WHFast**.

WHFast is a high-performance symplectic integrator designed for long-term gravitational simulations of planetary systems [31]. It is a modern, optimized implementation of the Wisdom–Holman mapping method, which separates the Hamiltonian of an N-body system into integrable Keplerian motion and perturbative interactions. Unlike the simpler leapfrog integrator, which operates on basic velocity and position updates, WHFast incorporates advanced techniques such as Hamiltonian splitting in Jacobi coordinates, an improved Kepler solver, and high-order symplectic correctors to significantly improve accuracy and efficiency. Its time-reversibility, unbiased

round-off error behavior, and good conservation of energy and angular momentum make WHFast suitable for long-term celestial mechanics problems [31].

The other integrator used, IAS15, is a 15th-order adaptive integrator based on Gauß–Radau quadrature, designed for extremely high-precision simulations of gravitational dynamics [32]. Unlike WHFast, which is a symplectic integrator optimized for nearly Keplerian motion and fixed timesteps, IAS15 is not symplectic, but achieves machine precision by carefully minimizing both systematic and floating-point errors. It supports arbitrary velocity-dependent and non-conservative forces, making it ideal for systems with close encounters, dissipative effects, or high-eccentricity orbits where symplectic integrators often struggle. Its use of adaptive time stepping, compensated summation, and predictor–corrector iterations allows IAS15 to conserve energy and angular momentum over billions of orbits, which few other integrators achieve. This makes IAS15 a powerful tool for long-term integrations in celestial mechanics with close encounters, where accuracy and stability are critical [32].

Both of these integrators were used throughout this project, but the main one used was IAS15 as that seemed to give the more accurate results, especially for more chaotic simulations with close encounters. Although I started to use Rebound just to confirm my own code, I made the choice to switch and use Rebound for the remainder of the project. This was mainly due to the fact that Rebound is easy to use, the simulations are faster than my code and that it is a very well-established software known to work well for orbital simulations.

3.1.2.2 Initial conditions

From this point onward, all simulations were performed in two dimensions, with the inclination i, argument of periapsis ω, and longitude of the ascending node Ω set to zero. This decision was motivated by two main factors. First, after extensive testing with various initial conditions, these parameters were found to have a comparatively minor effect on the system's evolution relative to other parameters. Second, fixing these values to zero significantly reduced computational time, allowing for a greater number of simulations to be performed more efficiently. The parameter θ, which determines the planet's initial position along its orbit, was also set to zero. This corresponds to both planets starting at $y = 0$ and a positive x value, with the exact position determined by their respective initial semi-major axes and eccentricities.

Henceforth, the simulations varied the mass, initial semi-major axis, and initial eccentricity of the third body. The time step, number of iterations, and choice of integrator were sometimes adjusted between simulations, depending on the particular aspect of the system under investigation. For instance, some simulations were extended with a greater number of iterations to study how the system evolved over longer timescales. In terms of parameter variation, the simulations were effectively divided into two phases. Initially, a broad parameter sweep was conducted over the ranges $0.1\ M_{Jup} \leq m \leq 30\ M_{Jup}$, $0.1\ \text{AU} \leq a \leq 15\ \text{AU}$, and $0 \leq e \leq 0.8$ in order to explore which regions of parameter space could potentially lead to the formation

of hot Jupiters. Based on the results of this exploratory phase, the parameter space was narrowed and subsequent simulations were carried out in a more targeted manner, with the goal of refining the conditions under which the desired outcomes were observed.

The primary objectives of these simulations were not only to produce hot Jupiters, but to do so in a physically plausible way. This naturally imposed some constraints on the initial conditions—particularly avoiding scenarios in which the third body started too close to Jupiter or with an unrealistically high initial eccentricity, as such configurations are not typically expected in real planetary systems.

3.1.2.3 Output

Using Rebound, I produced a large number of figures, each falling into one of three general categories: grid plots, scatter plots, and single-case plots showing orbital trajectories, eccentricities, and semi-major axes over time.

The first category consisted of grid plots. In all of these, the initial semi-major axis of the third body was plotted on the x-axis, while the mass of the third body was shown on the y-axis. To account for variations in the initial eccentricity, a separate grid plot was generated for each value of initial e. Each plot included a colormap and accompanying colorbar that visualized one of five different quantities: the final eccentricity of either Jupiter or the third body, the final semi-major axis of either Jupiter or the third body, or the final semi-major axis of Jupiter after incorporating the effects of tidal dissipation, as calculated using Equation 2.2.

The second type of figures were scatter plots. These displayed the final semi-major axis of Jupiter on the x-axis (using a logarithmic scale) and the final eccentricity of Jupiter on the y-axis. Each scatter plot also included a colormap and colorbar representing one of the following properties of the third body: its mass, its initial eccentricity, or its initial semi-major axis.

The final category consisted of single-case plots. Each case included five separate figures: the orbital trajectories of the planets, the evolution of eccentricity for both bodies over time, and the evolution of their semi-major axes over time. These plots served two main purposes. First, they made it possible to observe how key parameters evolved throughout the full duration of a simulation, in contrast to the grid and scatter plots which only visualized the final values. Second, since these simulations did not involve varying parameters, they allowed for finer time resolution and more iterations, making them particularly useful for analyzing the detailed dynamics of specific scenarios.

3.2 Comparison to observed planets and other research

As a final part of the project, I compared the results of my simulations to real planets that have been observed, as well as to other research papers that also have used simulations to try to probe Jupiters to become hot Jupiters through HETM.

To find the exoplanets, I used **astroquery** which is a software with a collection of tools to access data from different databases [33]. From astroquery I accessed the **NASA Exoplanet Archive**, which is an online database that provides a comprehensive and up-to-date collection of confirmed exoplanet discoveries and related stellar and planetary data, curated for use in scientific research [11][34].

Finally, the simulations and results of this project was compared to relevant literature to discuss differences and possible improvements to this project. The three scientific papers that was used for comparison were: Beaugé & Nesvorný (2012) [35], Buchhave et al. (2018) [36], and Banerjee et al. (2024) [37].

4

Results

In this section the results of the project are put forth and explained. The results include a comparison of simulations with my code and with Rebound, the most important figures produced during the project, and a comparison of my simulated results with observed planets.

4.1 My code vs Rebound

To test and try to confirm the accuracy of my code compared to that of Rebound with different integrators, many simulations were done. One set of typical results of such simulations are shown in the four figures below. For this simulation, the third body had a mass $m = 5.5\ M_{Jup}$ and initial semi-major axis $a = 7.55$ AU. Figure 4.1 was made using the Rebound code with the IAS15 integrator, however, creating the same figure with my code or with Rebound and the leapfrog integrator gave identical figures.

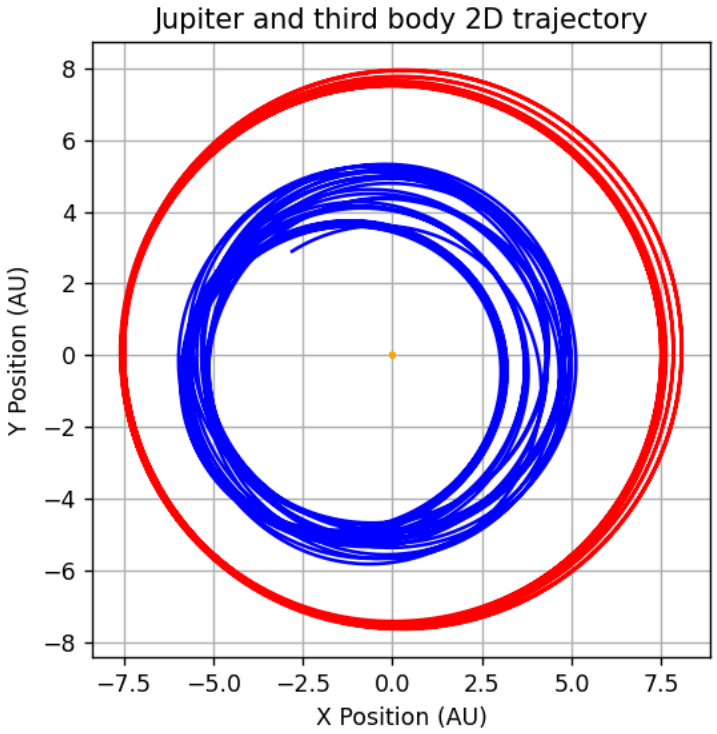

Figure 4.1: Orbits of the Jupiter (blue) and the third body (red) around a Sun-like star (yellow) over 100000 Earth days, with the third body's initial conditions being $m = 5.5\ M_{Jup}$ and $a = 7.55$ AU.

In figure 4.2 the simulation was done using my code and the total energy and angular momentum of the system is plotted over time. Since both of these quantities should be fully conserved in this system, the variation was calculated to assess the code's accuracy. The relative variation for this simulation using my code was 3.4×10^{-6} for the energy and 4×10^{-14} for the angular momentum.

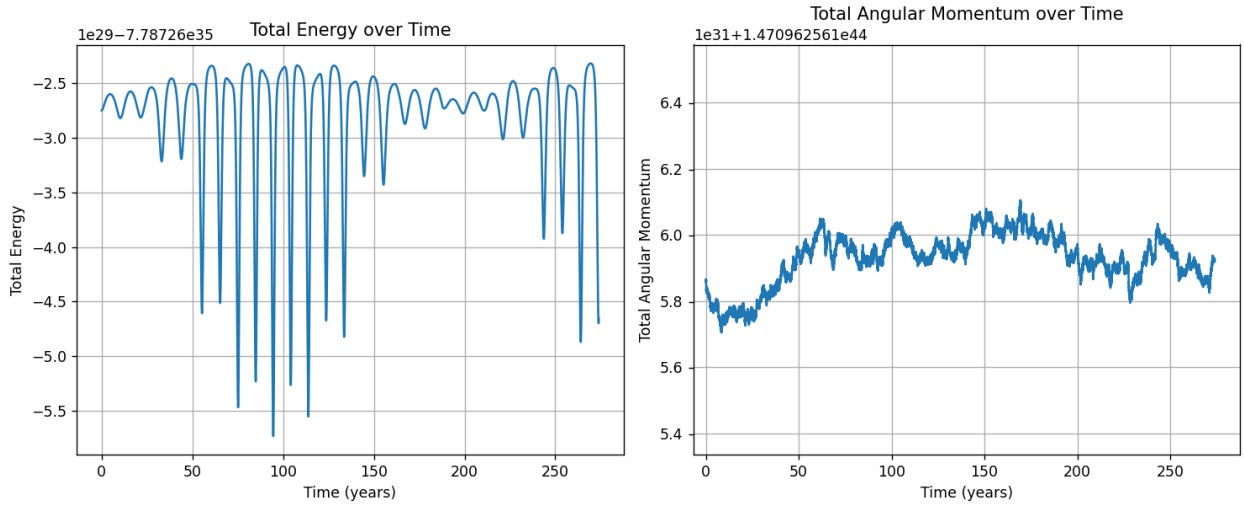

Figure 4.2: Left: The total energy of the system over time for the simulation in figure 4.1 using my code. Right: The total angular momentum of the system over time for the simulation in figure 4.1 using my code.

The same thing was done in figure 4.3 for the Rebound code with the leapfrog integrator. The relative variation for this model amounted to 1.5×10^{-6} for the energy and 3.6×10^{-14} for the angular momentum.

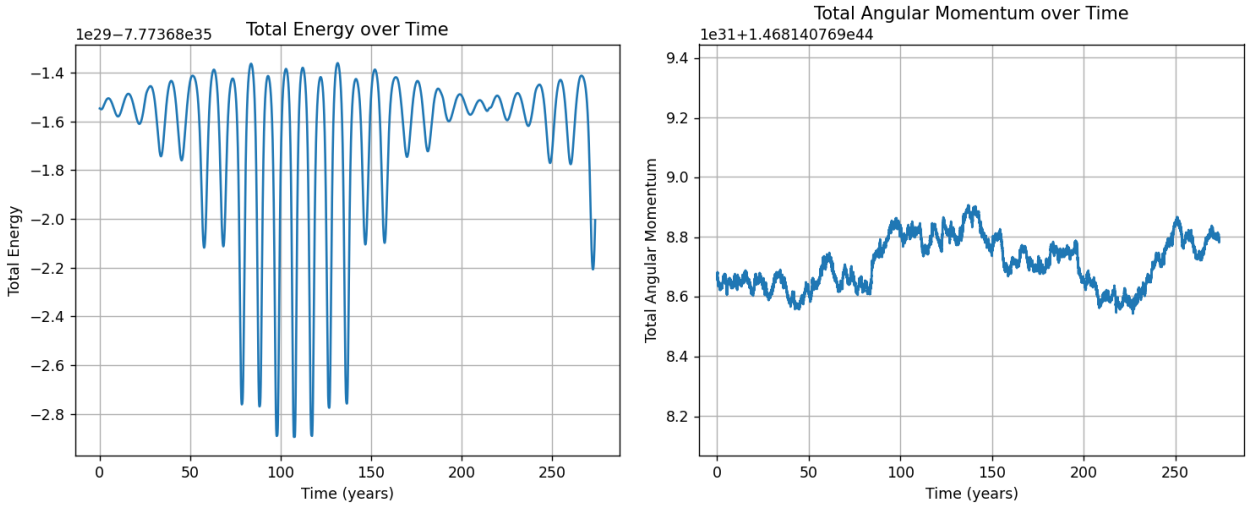

Figure 4.3: Left: The total energy of the system over time for the simulation in figure 4.1 using Rebound with the leapfrog integrator. Right: The total angular momentum of the system over time for the simulation in figure 4.1 using Rebound with the leapfrog integrator.

Once again the same process was done in figure 4.4 for the Rebound code but with the IAS15 integrator. The relative variation found in this model was 1.5×10^{-14} for the energy and 1×10^{-15} for the angular momentum.

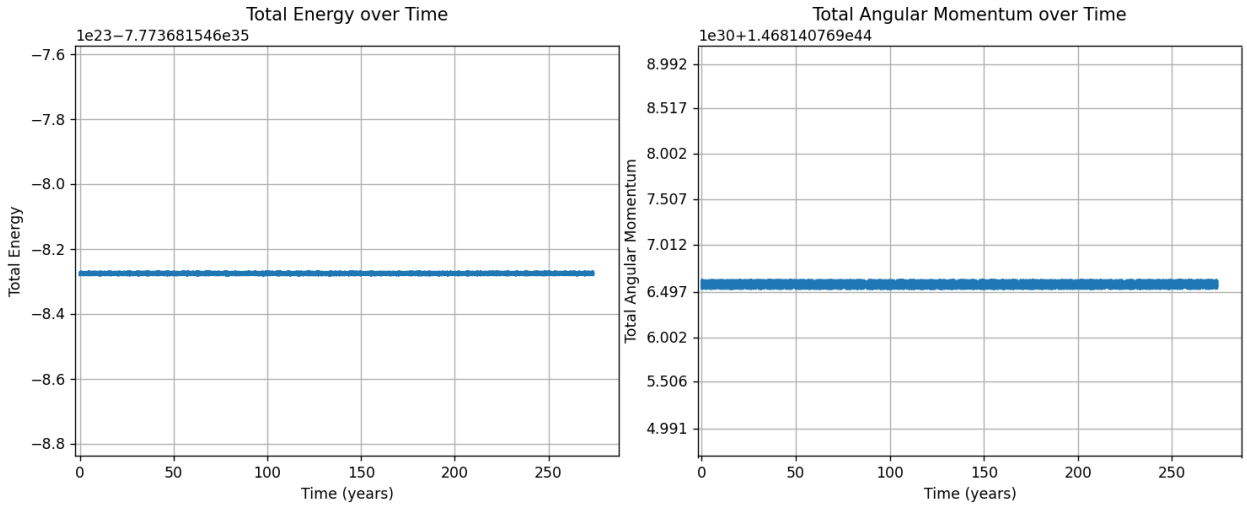

Figure 4.4: Left: The total energy of the system over time for the simulation in figure 4.1 using Rebound with the IAS15 integrator. Right: The total angular momentum of the system over time for the simulation in figure 4.1 using Rebound with the IAS15 integrator.

Comparing figures 4.2 and 4.4 and the relative variation between my code and the Rebound code with the leapfrog integrator, the difference is very small. This is good for my code since it is also built using the leapfrog algorithm, which therefore shows that my code can produce results that are consistent with those of Rebounds. However, comparing these results to the Rebound code using the IAS15 integrator, both the figures and relative variations are quite different. Regarding the relative variation in angular momentum, it is better but only by a factor of ~ 10. However the relative variation in the energy is better by about a factor of 10^8 which is a massive improvement. The figures along with the relative variations show both the energy and angular momentum to be more stable along the expected values, though some oscillations still occur.

4.2 Simulations

This section provides the main simulation results of the project and is divided into three parts according to what type of figures and simulations that were done.

4.2.1 Grid plots

One type of figure that was produced during the project is grid plots. Figure 4.5 shows four grid plots, each with a different initial eccentricity of the third body, but their third body mass and semi-major axis varied over the same range. In figure 4.7, the same simulation was done as in figure 4.5 but with four higher initial eccentricities. These figures show the case where the third body starts off closer to the Sun than the Jupiter. The black points in these figures are systems where the Jupiter eccentricity is above 1, meaning that the Jupiter has been ejected from its system. Analyzing these figures, it is apparent that the final eccentricity of Jupiter

depends on each of the varying parameters. The mass of the third body seems to not be that important as long as it is over a few Jupiter masses, but if it is lower than about 1 Jupiter mass, it drastically reduces the effect on the Jupiters eccentricity. For the semi-major axis there is a quite clear line that separates the cases where Jupiter's eccentricity is affected or not, which shows that the two planets have to be within a certain distance of each other to excite the eccentricity of Jupiter. The initial eccentricity of the third body also clearly affects the Jupiters eccentricity in the sense that the higher the initial eccentricity, the further the third body can be from the Jupiter and still induce a higher eccentricity in Jupiter.

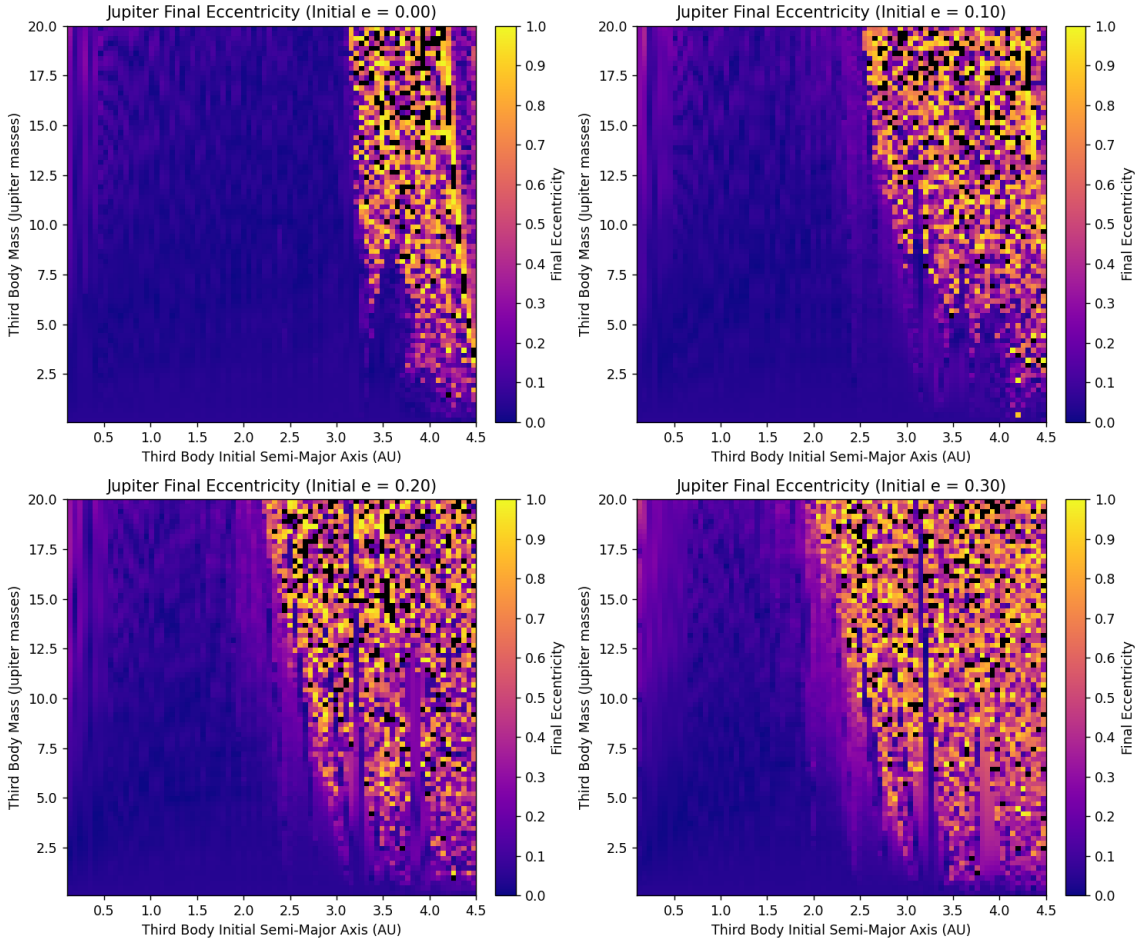

Figure 4.5: A simulation with Rebound and the IAS15 integrator showing the final eccentricity of the Jupiter as a colormap for systems with the following initial conditions: 10 days time step, 20000 iterations per system, the third body's mass and semi-major axis varying 80 times each over 0.1 $M_{Jup} \leq m \leq 20\ M_{Jup}$ and 0.1 AU $\leq a \leq$ 4.5 AU, and the third body's eccentricity varying 4 times over $0 \leq e \leq 0.3$.

In figures 4.6 and 4.8 which corresponds to the simulations for figures 4.5 and 4.7 respectively, the tidal dissipation was calculated with the final eccentricity and semi-major axis of the Jupiter using equation 2.2. These figures therefore show what each Jupiter orbit would look like after fully going through tidal dissipation and having

its eccentricity reduced to 0. The figures were plotted in a way such that the Jupiters that did not end up with a semi-major axis of below 1 after tidal dissipation were made gray. This was done to emphasize the systems that could possibly produce hot or warm Jupiters. They clearly show that the Jupiter needs to have a high eccentricity before undergoing tidal dissipation to have a chance of becoming a hot Jupiter. The most important thing to notice in these figures is that the amount of hot or warm Jupiters that can be produced, increases a lot as the initial eccentricity of the third body is increased.

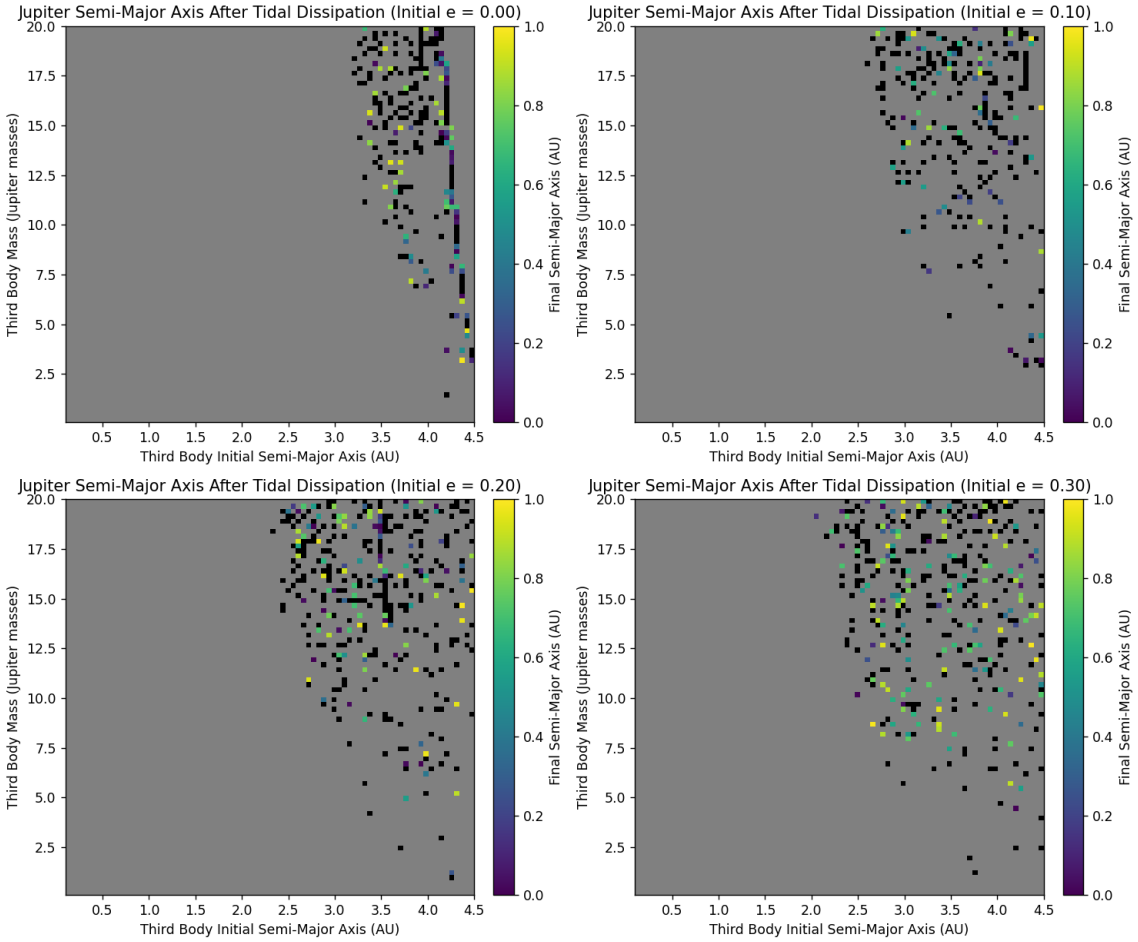

Figure 4.6: The same simulation as for figure 4.5 but with tidal dissipation accounted for in each system using equation 2.2.

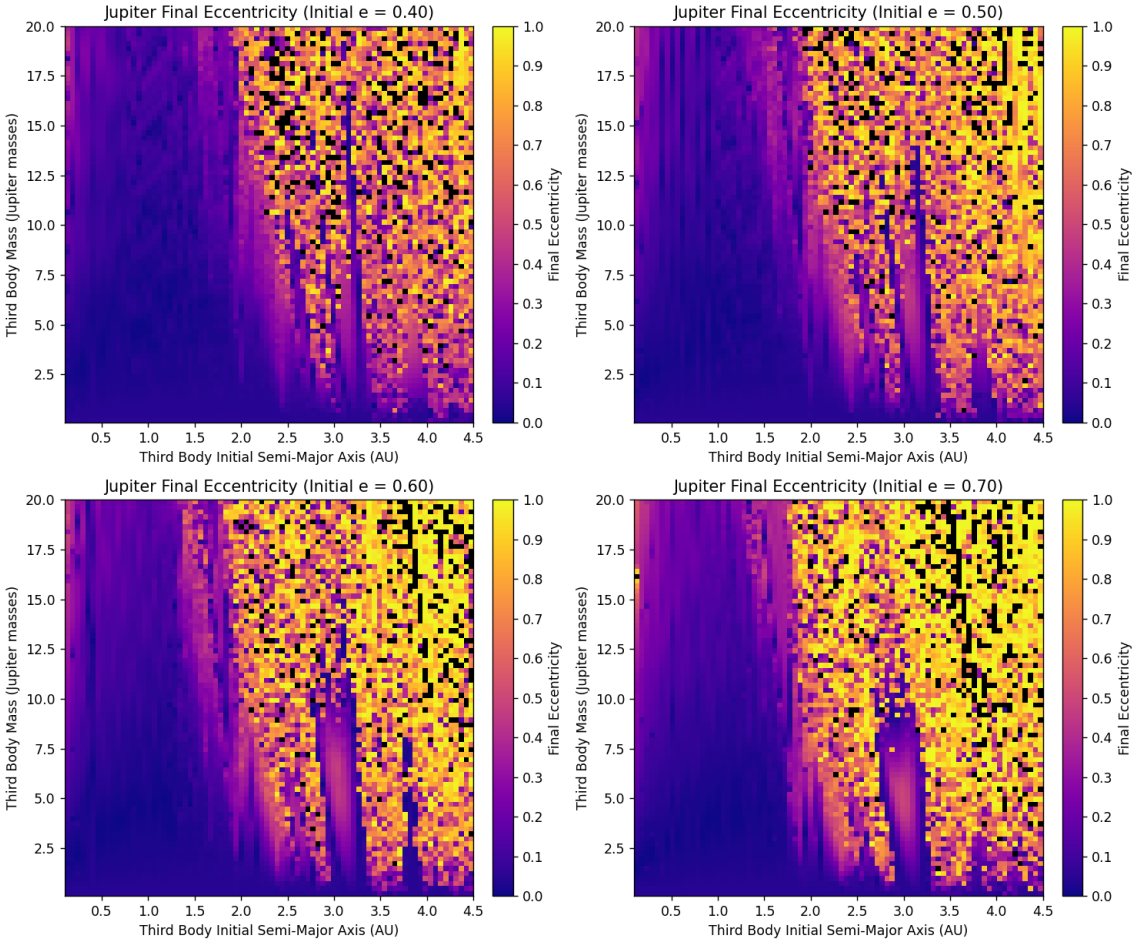

Figure 4.7: A simulation with Rebound and the IAS15 integrator showing the final eccentricity of the Jupiter as a colormap for systems with the following initial conditions: 10 days time step, 20000 iterations per system, the third body's mass and semi-major axis varying 80 times each over 0.1 $M_{Jup} \leq m \leq 20\ M_{Jup}$ and 0.1 AU $\leq a \leq$ 4.5 AU, and the third body's eccentricity varying 4 times over $0.4 \leq e \leq 0.7$.

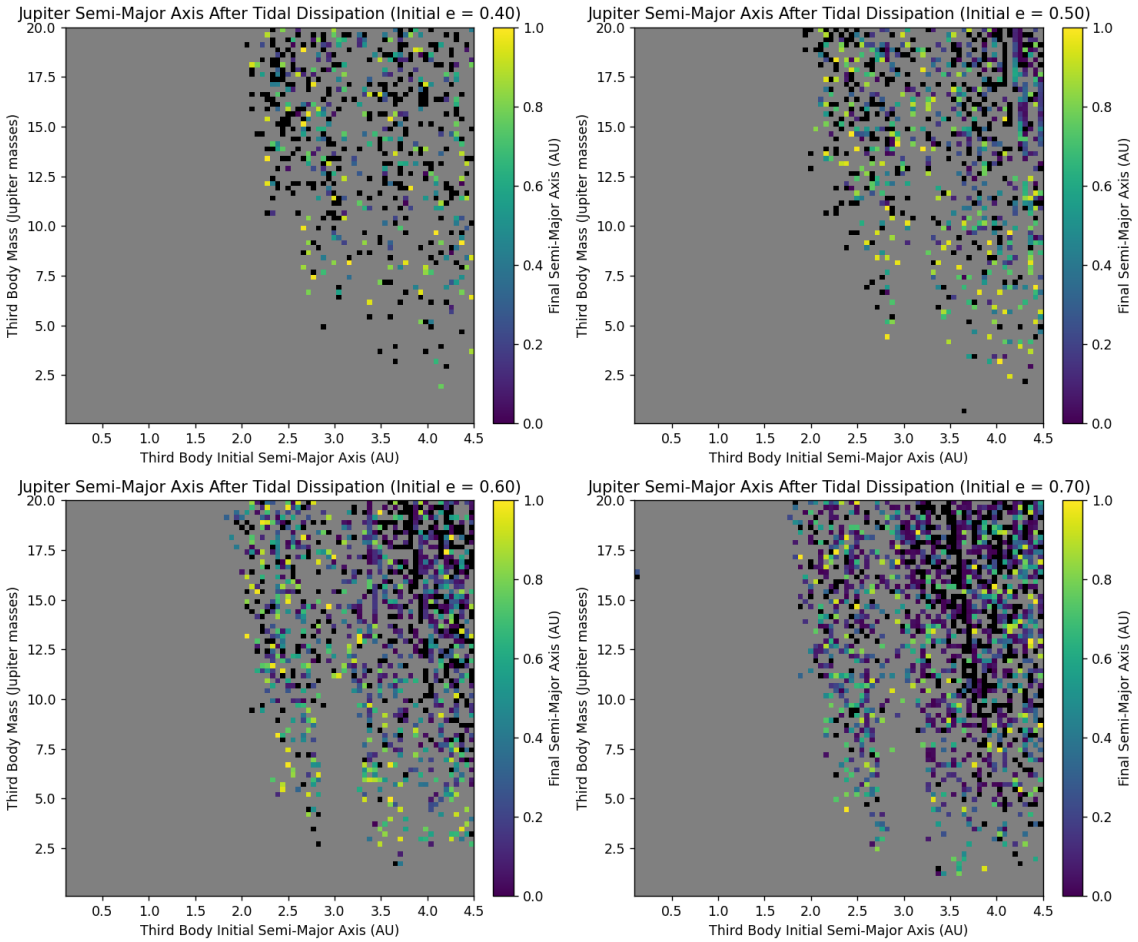

Figure 4.8: The same simulation as for figure 4.7 but with tidal dissipation accounted for in each system using equation 2.2.

In figure 4.9 a single grid plot is shown where the initial eccentricity for the third body is 0.7 in all systems. A difference between this simulation and the previous ones is that this simulation takes into account collisions between the bodies which the previous simulations did not. This means that if the planets in a system collide with each other, the simulation for this system stops and does not include it in the resulting data. The systems that had collisions were therefore plotted as white points in the figure. One thing to notice in figure 4.9 is the white "line" at just above 16 AU. That is there because the starting point of the Jupiter and the third body is at the roughly the same place here, meaning that they very easily collide with each other. Left of this line is thus the case where the third body starts closer to the Sun than the Jupiter, and right of this line is the case where the third body starts further away from the Sun than the Jupiter. The fact that this happens at above a semi-major axis of 16 AU and not at $a \approx 5.2$ AU (where the Jupiter starts) is because of the high initial eccentricity of 0.7 of the third body. The figure shows a lot of high final eccentricities of the Jupiter, especially above $5 - 10$ M_{Jup}. There are also more systems than anywhere else just left and right of the white line where the Jupiter is ejected from the system. This is logical since the planets gravitational effect on each other are the strongest here because of the short distance between

them.

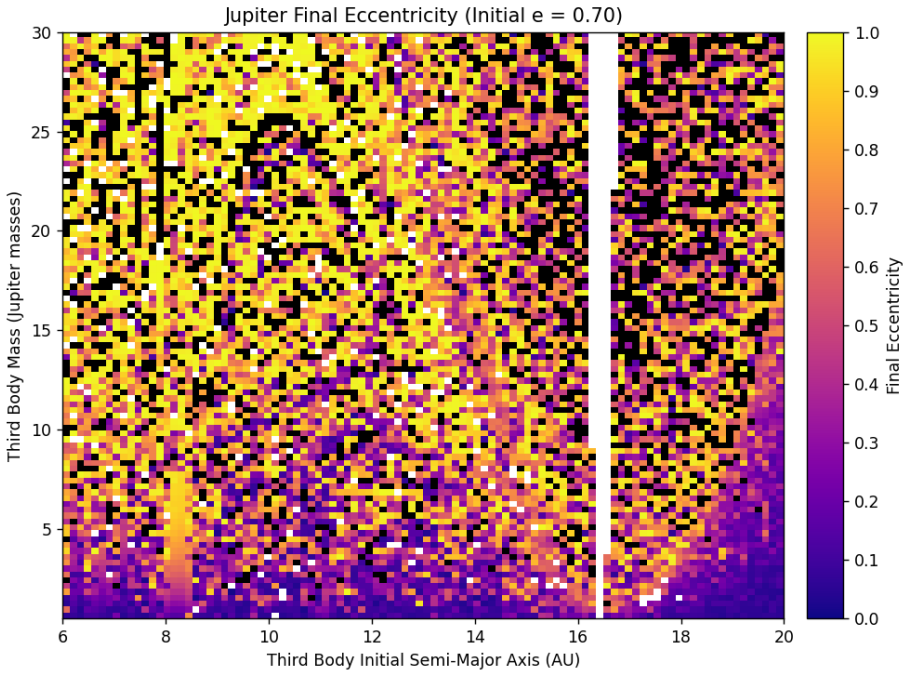

Figure 4.9: A simulation with Rebound and the IAS15 integrator showing the final eccentricity of the Jupiter as a colormap for systems with the following initial conditions: 10 days time step, 20000 iterations per system, the third body's mass and semi-major axis varying 100 times each over 0.5 $M_{Jup} \leq m \leq 30\ M_{Jup}$ and 6 AU $\leq a \leq$ 20 AU, and the third body's eccentricity $e = 0.7$.

The next two figures 4.10 and 4.11 are two simulations that are identical except for the latter one being run for 200 times more iterations for each system. These together are included to show the dependence on time of the simulations. Each of these simulations show the case where the third body starts out further from the Sun than the Jupiter, with the third body having 0 initial eccentricity.

The plots show that when increasing the time spent running for the simulations, the amount of high eccentricity Jupiters is increased, which is what is wanted. However, along with the high eccentricity Jupiters also come a large increase of systems where either the Jupiter is ejected or where the planets collide. The amount of systems that collided in the shorter simulation was calculated to be 158 out of a total of 1600 (9.88%). In the longer simulation, the amount of systems with a collision was 447 out of 1600 (27.94%). This is almost 3 times as many collisions as the shorter case, and a significant portion of the total systems where collisions happened.

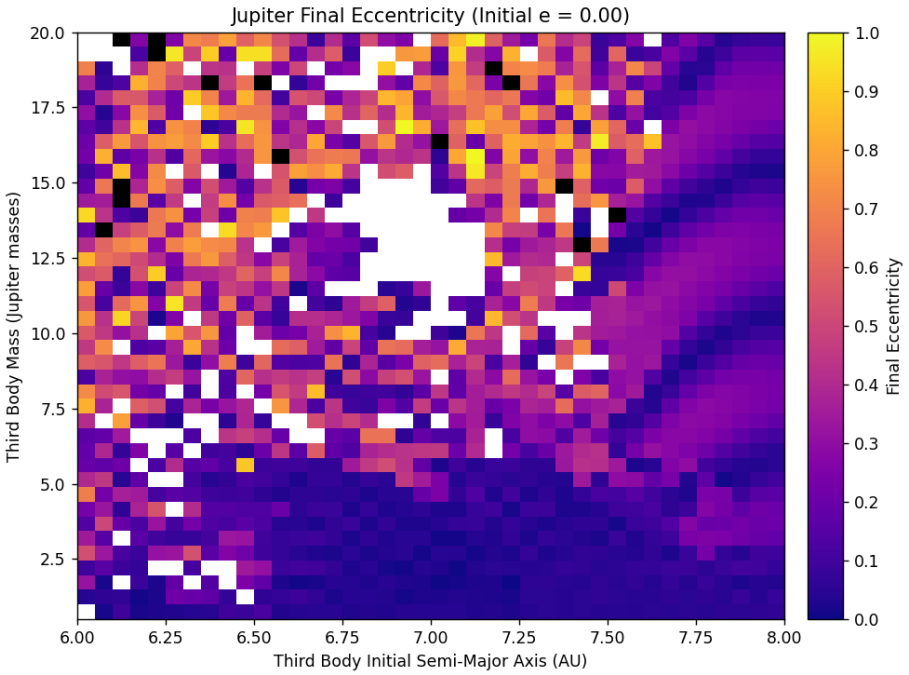

Figure 4.10: A simulation with Rebound and the IAS15 integrator showing the final eccentricity of the Jupiter as a colormap for systems with the following initial conditions: 10 days time step, 20000 iterations per system, the third body's mass and semi-major axis varying 40 times each over $0.5\ M_{Jup} \leq m \leq 20\ M_{Jup}$ and $6\ \text{AU} \leq a \leq 8\ \text{AU}$, and the third body's eccentricity $e = 0.0$.

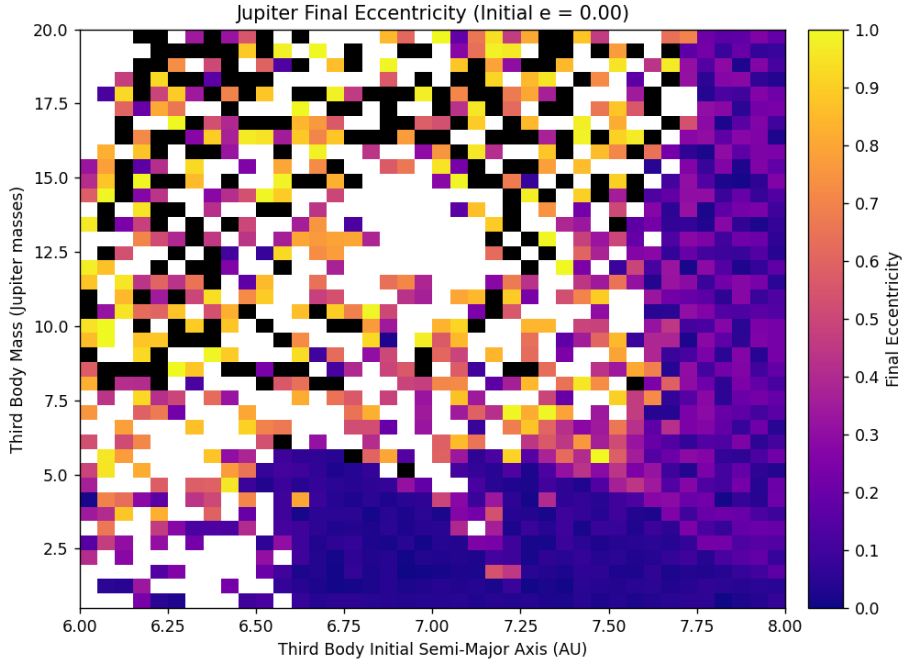

Figure 4.11: A simulation with all the same initial conditions as figure 4.10 except for having 4000000 iterations per system instead.

4.2.2 Scatter plots

Another type of figures that were produced in this project are scatter plots. Each of the scatter plots shown in this section compare the final eccentricity of the Jupiter to the final semi-major axis of the Jupiter, with an accompanying colormap for either Third body mass or initial semi-major axis. Figure 4.12 was created using the same data as figure 4.10. This figure clearly shows two tracks where almost all of the Jupiters reside. As the Jupiter increases its eccentricity, it either increases its semi-major axis a lot, or it decreases its semi-major axis slightly. The colormap of this figure also shows how the Jupiters' final values depends on the third body's mass. It's clearly visible that the majority of Jupiters with higher eccentricities in both tracks are in systems with a third body mass in the upper range of the spectrum. Whereas the systems with a lower third body mass tends to not increase the eccentricity of the Jupiter as much.

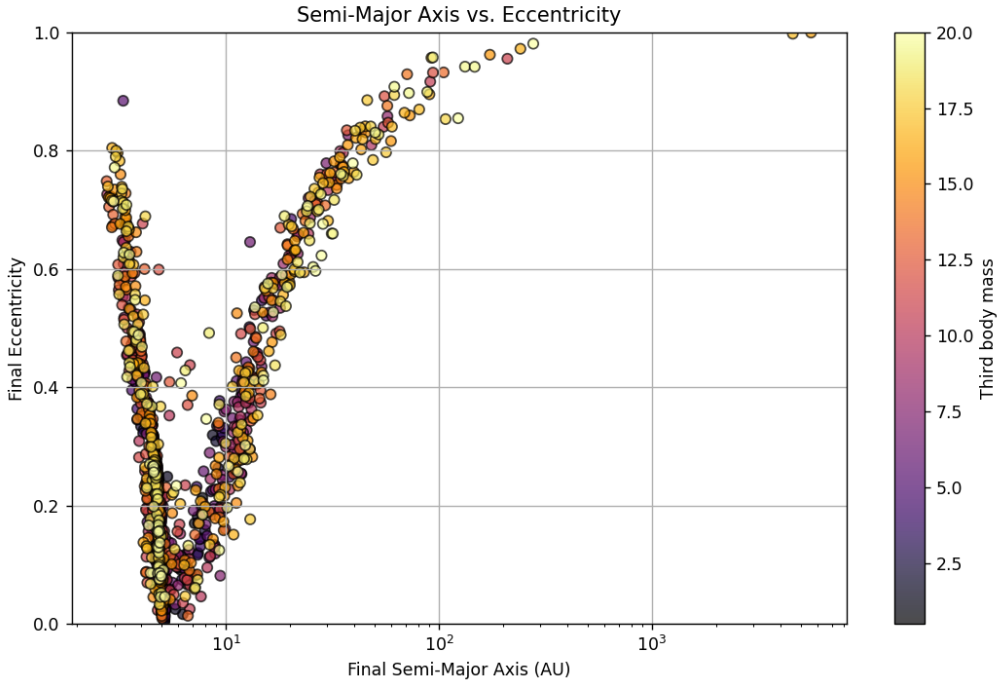

Figure 4.12: The same data as for figure 4.10 showing the Jupiter's final eccentricity on the y-axis and it's final semi-major axis on the x-axis (logarithmic scale), along with a colormap for the third body's mass.

Figure 4.13 and 4.14 shows two scatter plots which were created using the same data as figure 4.11, i.e. they have the exact same initial conditions as figure 4.12 but are run for 200 times longer. Comparing the shorter and longer run time figures it is clear that the general shape of the figures are very similar. One difference in shape is that figure 4.13 and 4.14 have quite a bit more Jupiters with very high eccentricity and semi-major axis. Another difference is that the gap between the left and right track is basically empty for the longer run time plots, whereas the shorter run time plot had some Jupiters in between the tracks. Figure 4.13 have a similar distribution of the third body mass as figure 4.12, but it shows some more lower third body mass

systems that end up with higher Jupiter eccentricities in both tracks. Figure 4.14 provides two main pieces of information about the dependence of the third body initial semi-major axis. Firstly, the systems with the highest initial semi-major axis very rarely end the simulation with a highly eccentric Jupiter, and they are mostly in the left track with a semi-major axis similar to what it started with. Secondly it shows that the lower initial semi-major axis systems tend to favor the right track above the left.

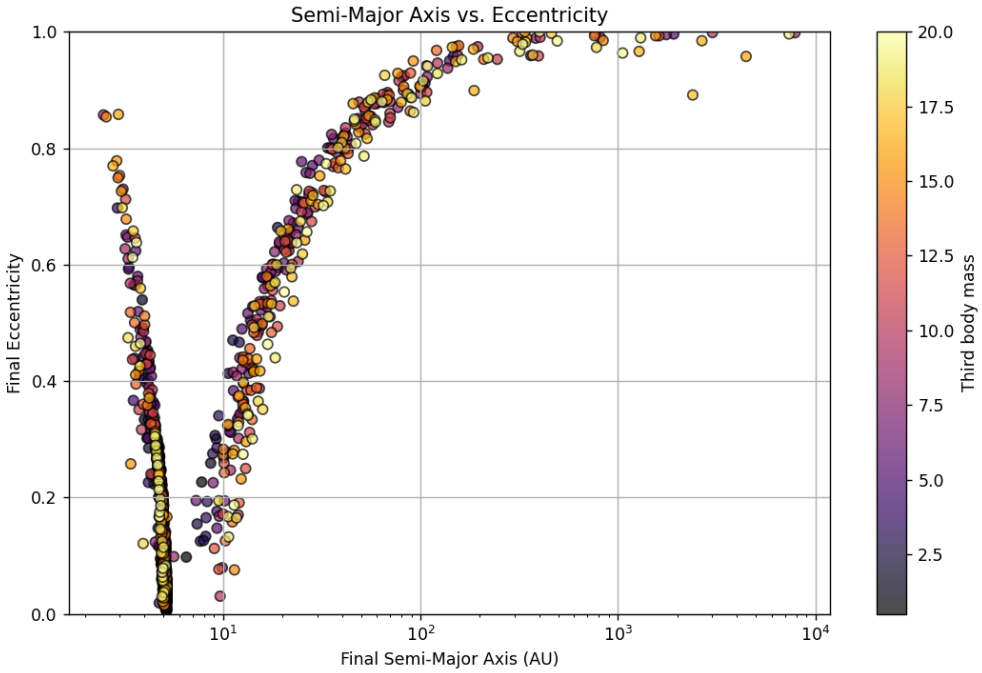

Figure 4.13: The same data as for figure 4.11 showing the Jupiter's final eccentricity on the y-axis and it's final semi-major axis on the x-axis (logarithmic scale), along with a colormap for the third body's mass.

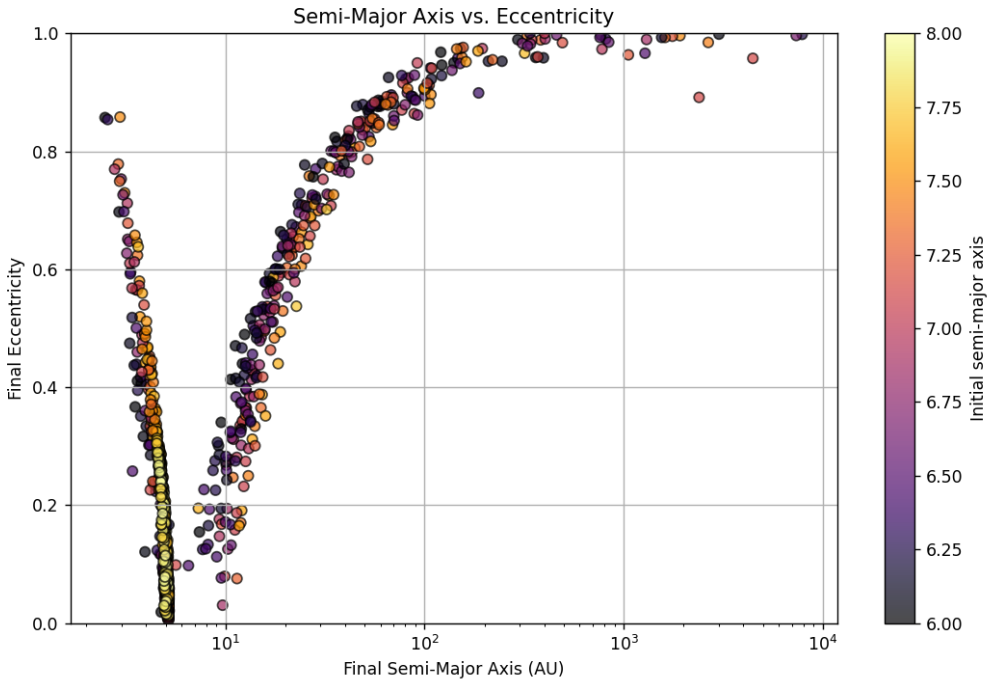

Figure 4.14: The same as figure 4.13 but with a colormap for the third body's initial semi-major axis.

The next scatter plots, figures 4.15 and 4.16, showcases the systems with the third body starting off closer to the Sun than the Jupiter and with an eccentricity of 0.7. Compared to the previous scatter plots, these two do not have any tracks that they follow, and their shape instead look a lot more random. From figure 4.15 it is hard to draw many conclusions on the dependence of third body mass, but one thing to note is that the absolute highest Jupiter eccentricities ($e \gtrsim 0.95$) all have a very high third body mass. From figure 4.16 a big thing to note is that the systems with the lowest initial third body semi-major axes, almost all have a very tiny effect on the Jupiters semi-major axis and none of them produce a very high eccentricity of the Jupiter.

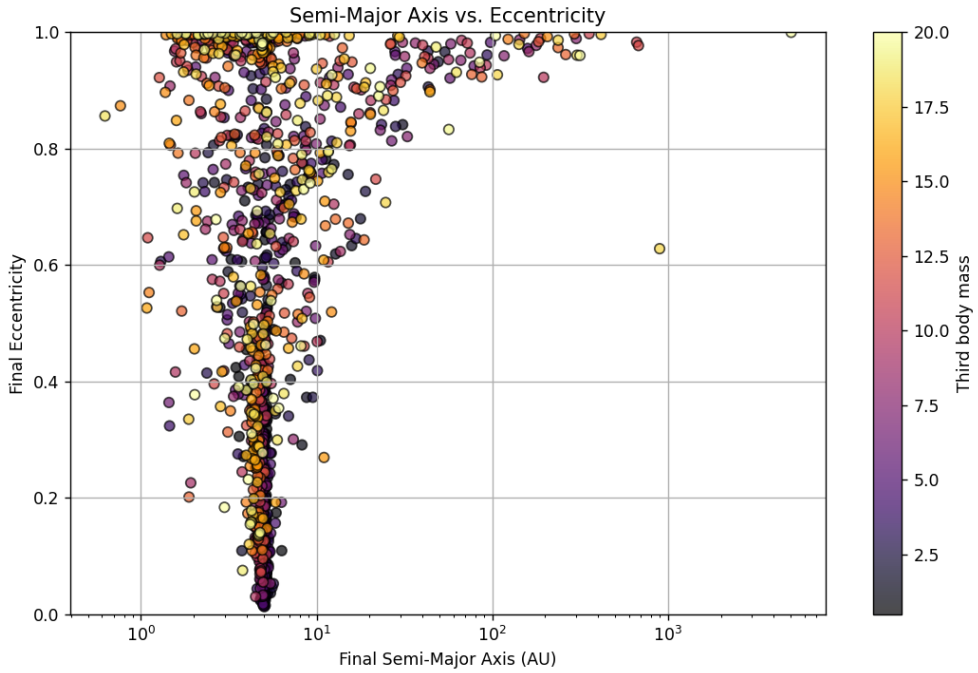

Figure 4.15: A simulation with Rebound and the IAS15 integrator showing the Jupiter's final eccentricity on the y-axis and it's final semi-major axis on the x-axis (logarithmic scale), along with a colormap for the third body's mass. The initial conditions were: 10 days time step, 200000 iterations per system, the third body's mass and semi-major axis varying 40 times each over $0.5\ M_{Jup} \leq m \leq 20\ M_{Jup}$ and $1\ \text{AU} \leq a \leq 5\ \text{AU}$, and the third body's eccentricity $e = 0.7$.

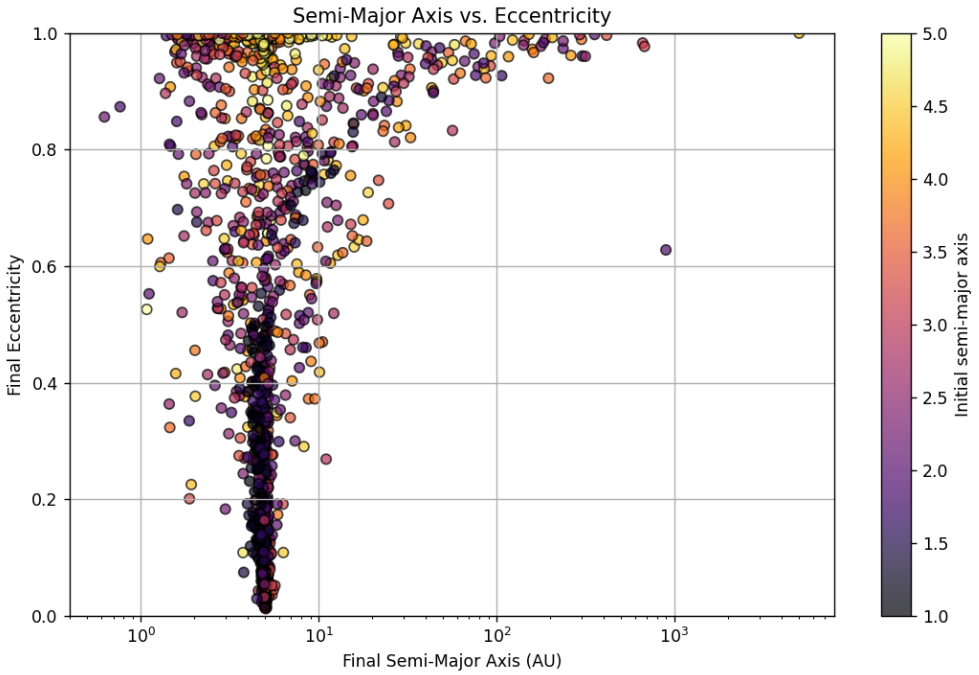

Figure 4.16: The same as figure 4.15 but with a colormap for the third body's initial semi-major axis.

Figure 4.17 shows the same data as for figure 4.9 but as a scatter plot with a colormap of the initial semi-major axis of the third body. The shape of the figure shows neither different tracks nor very randomly spread out data points, but instead show more evenly distributed values. Regarding how the third body's initial semi-major axis affects the Jupiter, the lower values clearly produce Jupiters with a lower final semi-major axis, while higher values seem to give Jupiters with more spread out and larger semi-major axes.

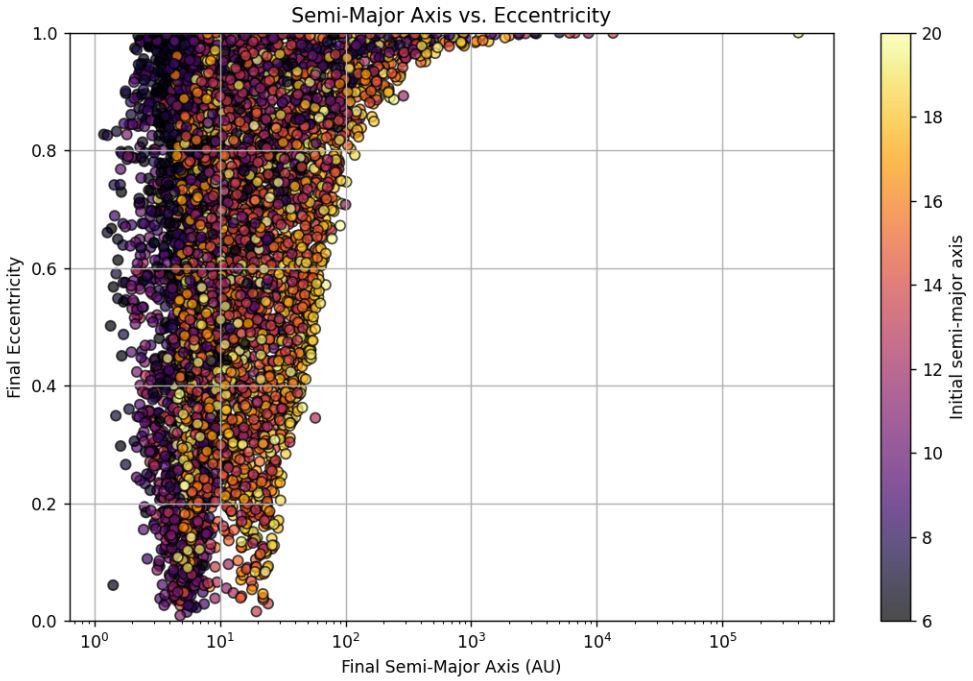

Figure 4.17: A simulation with Rebound and the IAS15 integrator showing the Jupiter's final eccentricity on the y-axis and it's final semi-major axis on the x-axis (logarithmic scale), along with a colormap for the third body's semi-major axis. The initial conditions were: 10 days time step, 20000 iterations per system, the third body's mass and semi-major axis varying 100 times each over 0.5 $M_{Jup} \leq m \leq$ 30 M_{Jup} and 6 AU $\leq a \leq$ 20 AU, and the third body's eccentricity $e = 0.7$.

4.2.3 Single-case plots

While the grid plots and scatter plots in the previous sections are great to get an overview of a lot of systems with many different initial conditions, the following figures look at single system simulations to see how the planets actually get to their final eccentricity and semi-major axis values. Out of the many simulations of testing carried out in this project, some were chosen to take a closer look at for different reasons.

From a simulation done for a large amount of systems with an initial third body semi-major axis, eccentricity and mass that all were varied, ten systems with a high final Jupiter eccentricity and Jupiter semi-major axis were chosen to be plotted individually. All of the results for these cases were very similar with a typical result shown in figure 4.18. In this figure as well as the others not shown here, the Jupiter orbits the Sun while being affected by the third body until at one point when the planets have a close encounter, the Jupiter gets slung out in a highly eccentric orbit with a very big semi-major axis.

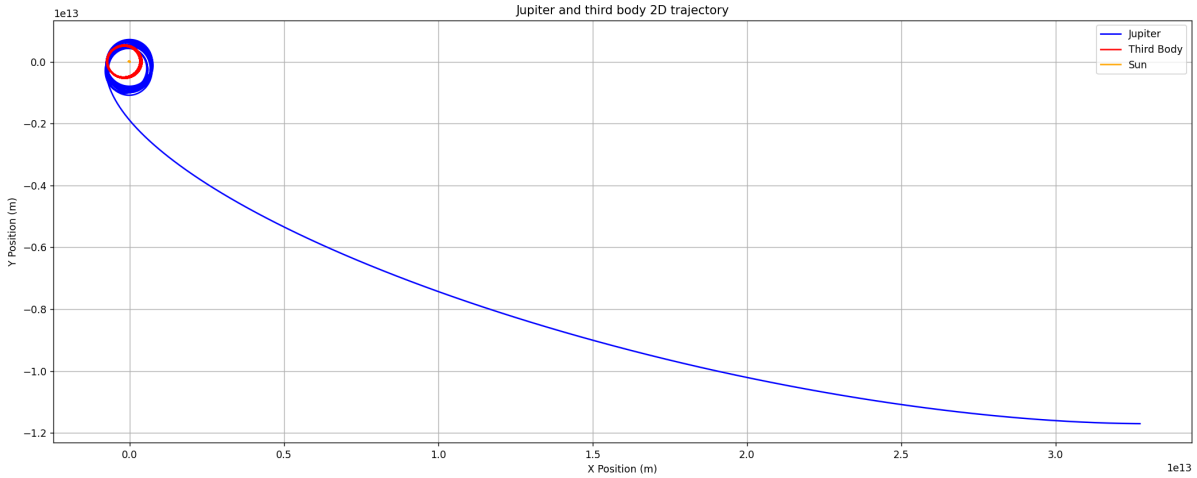

Figure 4.18: Orbits of a system simulated with Rebound and the IAS15 integrator, with the third body's initial conditions being $m = 17.985\ M_{Jup}$, $a = 3.776$ AU and $e = 0.3$.

Next, from a large simulation done for systems where the third body started inside of the Jupiter with an eccentricity of 0.3 or lower in each system, ten systems that ended with a fairly high eccentricity and a low semi-major axis were chosen. Out of these systems, one such typical result is seen in figure 4.19. It shows a simulation where the third body is almost stable in its orbit, but the Jupiter's orbit is very chaotic. Even though the simulation ends up with a high eccentricity and low semi-major axis which is the desired outcome to create hot Jupiters, the chaotic nature of the orbit makes it so that there is no guarantee that the Jupiter will stay in a similar orbit for a long period of time.

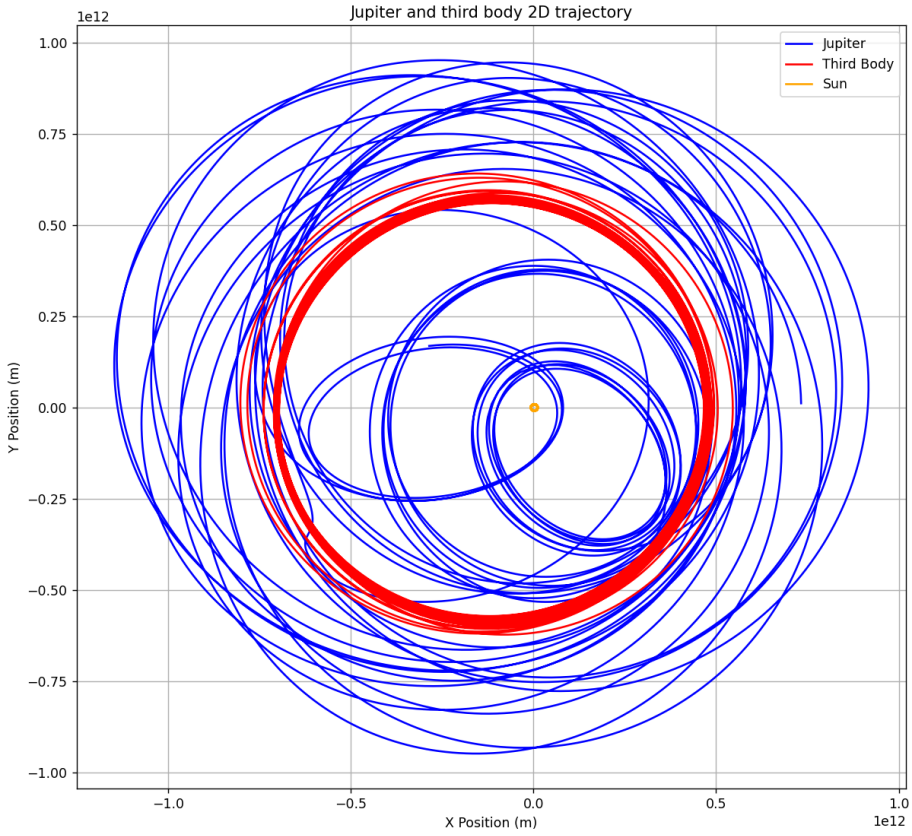

Figure 4.19: Orbits of a system simulated with Rebound and the IAS15 integrator, with the third body's initial conditions being $m = 15.970\ M_{Jup}$, $a = 3.999$ AU and $e = 0.2$.

The next figure is from a large simulation of systems with a third body initial eccentricity that varied between $0.4 \leq e \leq 0.7$. From this simulation, 15 systems were chosen that ended up with a Jupiter with a small semi-major axis and a large eccentricity, and a typical such result is shown in figure 4.20. The orbit of this Jupiter is somewhat similar to the last figure 4.19. But in this figure, and typically the other ones chosen for this simulation as well, the Jupiter's orbit is overall a little less chaotic.

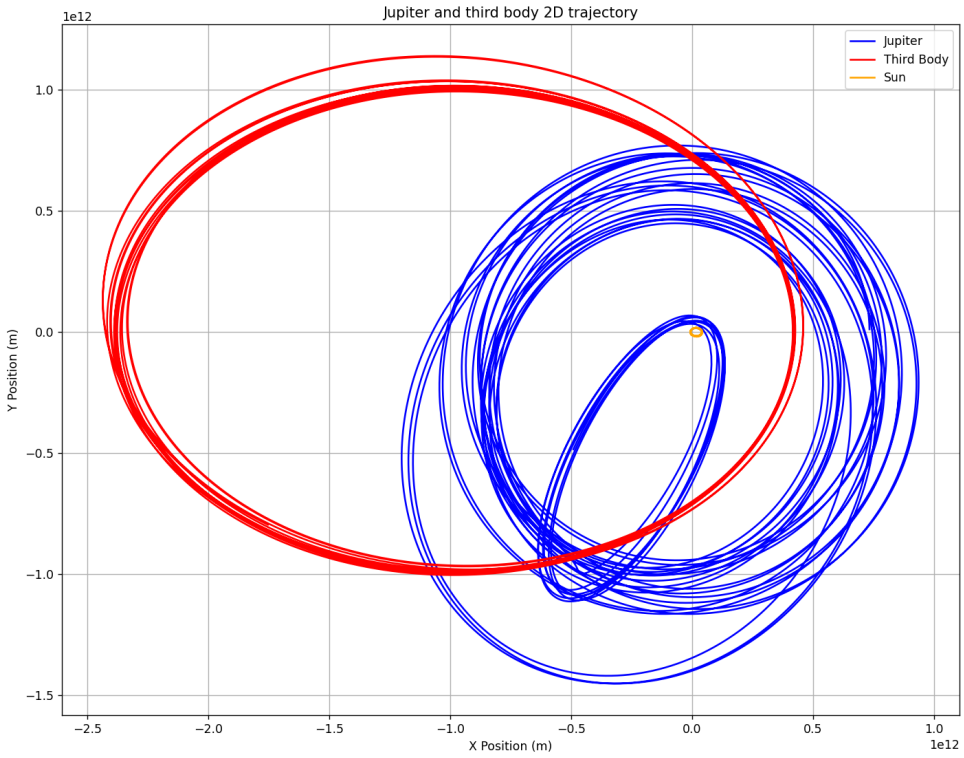

Figure 4.20: Orbits of a system simulated with Rebound and the IAS15 integrator, with the third body's initial conditions being $m = 17.733\ M_{Jup}$, $a = 9.532$ AU and $e = 0.7$.

The previous figures looked at simulations that ended up in high eccentric orbits at the final point in their simulations. The next figures will look in to Jupiters that did not end up at high eccentric orbits at the end of their simulations, and instead run the simulation a lot longer to see if there is an indication that they could evolve after a long time.

The next three figures were chosen from the simulation done in 4.11, specifically from the blue and purple areas at the edges where it seems that nothing happens to the Jupiter eccentricity. Since these simulations were run for such a long time, it was not possible to plot the orbits themselves, but instead the plots of the Jupiters' eccentricity and semi-major axes over time are shown instead. The first plot, figure 4.21, is from the blue area and was run for 100 times longer than in its original simulation (100 million years). It shows that nothing changes no matter how long the simulation is run for.

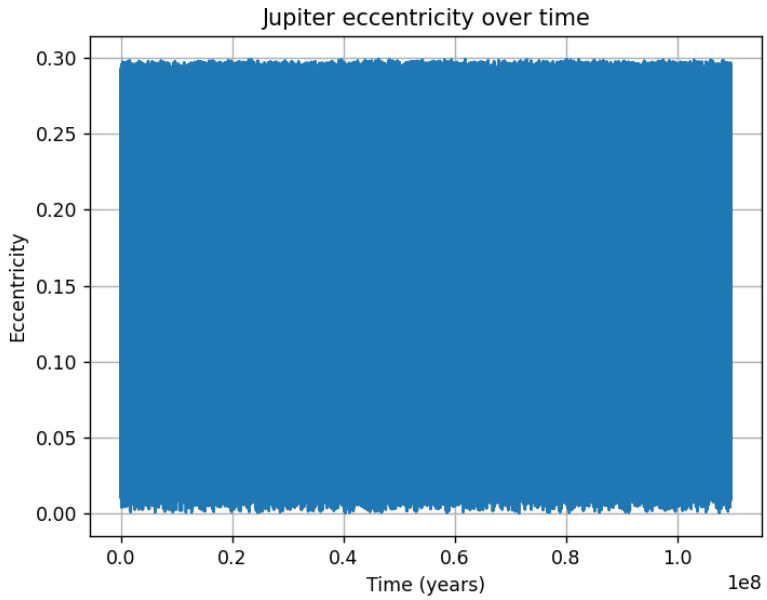

Figure 4.21: A simulation with Rebound and the IAS15 integrator for a single system showing the Jupiter's eccentricity over time with initial conditions: 10 days time step, 4×10^9 iterations, third body's mass, semi-major axis, and eccentricity $m = 7\ M_{Jup}$, $a = 7.8$ AU, $e = 0.0$.

Figure 4.22 was chosen from a bit more purple area in figure 4.11 closer to the edge to try to get something more to happen than in figure 4.21. This figure shows a lot more happening than in the previous figure, but it is not what is wanted. Up until about 40000 years, it seems to be on a path towards a high eccentricity and low semi-major axis, but then this is disrupted and instead starts oscillating with neither very high eccentricities nor low semi-major axes. One thing to note is that this simulation was run for the same amount of iterations as figure 4.21 but it only gives a timescale of just over 100 thousand years, almost 1000 times less than the previous figure. This is due the nature of the IAS15 integrator which reduces the time step when planets get closer to each other to retain the accuracy of the simulation.

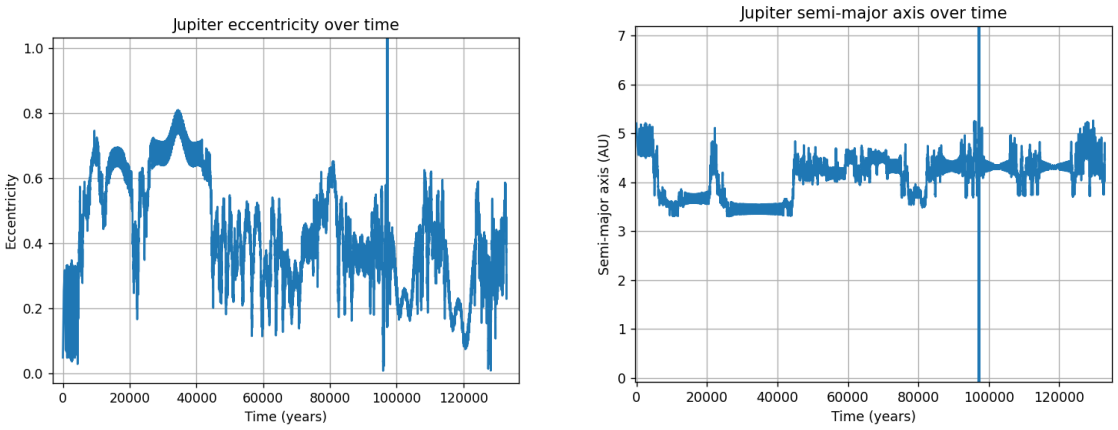

Figure 4.22: Left: A simulation with Rebound and the IAS15 integrator showing the Jupiter's eccentricity over time with the initial conditions: 10 days time step, 4×10^8 iterations, third body's mass, semi-major axis, and eccentricity $m = 5.5\ M_{Jup}$, $a = 7.55$ AU, $e = 0.0$. Right: The same simulation as the left but showing the Jupiter's semi-major axis over time.

In figure 4.23, the exact same simulation was run as for figure 4.22 but using the WHFast integrator instead of IAS15. This was done to see how much of an effect the choice of integrator had. These figures are similar in their overall shape with a lot of oscillations and a few places that look a little more stable. However, the details of the orbits and where they end up at the end of the simulation is very different. This means that the choice of integrator and length of time step is very important to be able to have a good enough accuracy to trust the results.

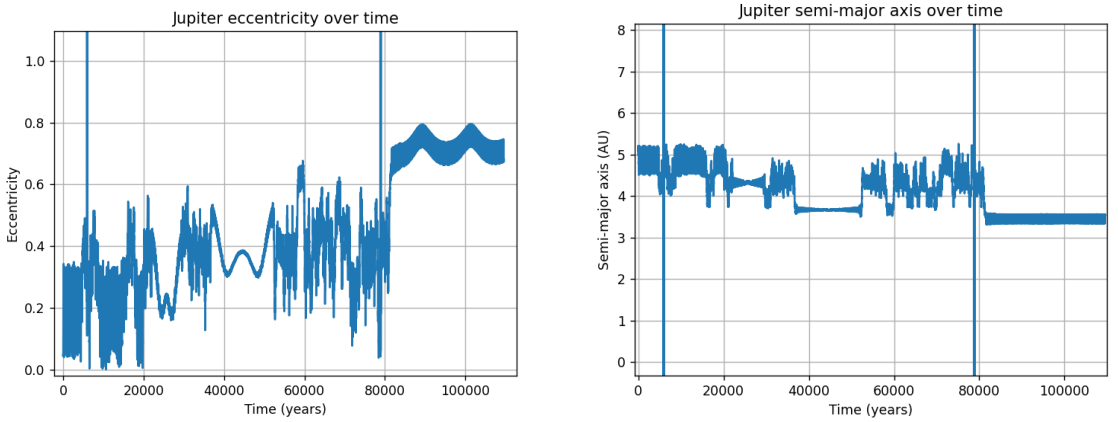

Figure 4.23: Left: A simulation with Rebound and the WHFast integrator showing the Jupiter's eccentricity over time with the initial conditions: 0.1 days time step, 4×10^8 iterations, third body's mass, semi-major axis, and eccentricity $m = 5.5\ M_{Jup}$, $a = 7.55$ AU, $e = 0.0$. Right: The same simulation as the left but showing the Jupiter's semi-major axis over time.

4.3 Observed planets

To better understand what types of orbits are sought after in this project and to see what the distribution of real observed planets looks like in relation to this, figure 4.24 is provided. This figure shows all planets that have been observed with a semi-major axis of 0.01 AU $\leq a \leq$ 5 AU and a mass of 0.5 $M_{Jup} \leq m \leq$ 10 M_{Jup} according to the NASA Exoplanet Archive [34]. The gray region in this figure is an approximate track which follows $a_{final} = a(1 - e^2) =$ constant, that a planet has to be on to be able to go through HETM. The limits of this migration process are physically constrained. The right limit of $a_{final} = 0.1$ AU is set by the tidal circularization timescale which corresponds to the maximum eccentricity that can be reached before tidal dissipation becomes efficient enough to circularize the orbit [22]. This is primarily set by the planet's tidal Q value and structure. The left limit of $a_{final} = 0.034$ AU is set by the Roche limit, inside of which a planet would be tidally disrupted [22].

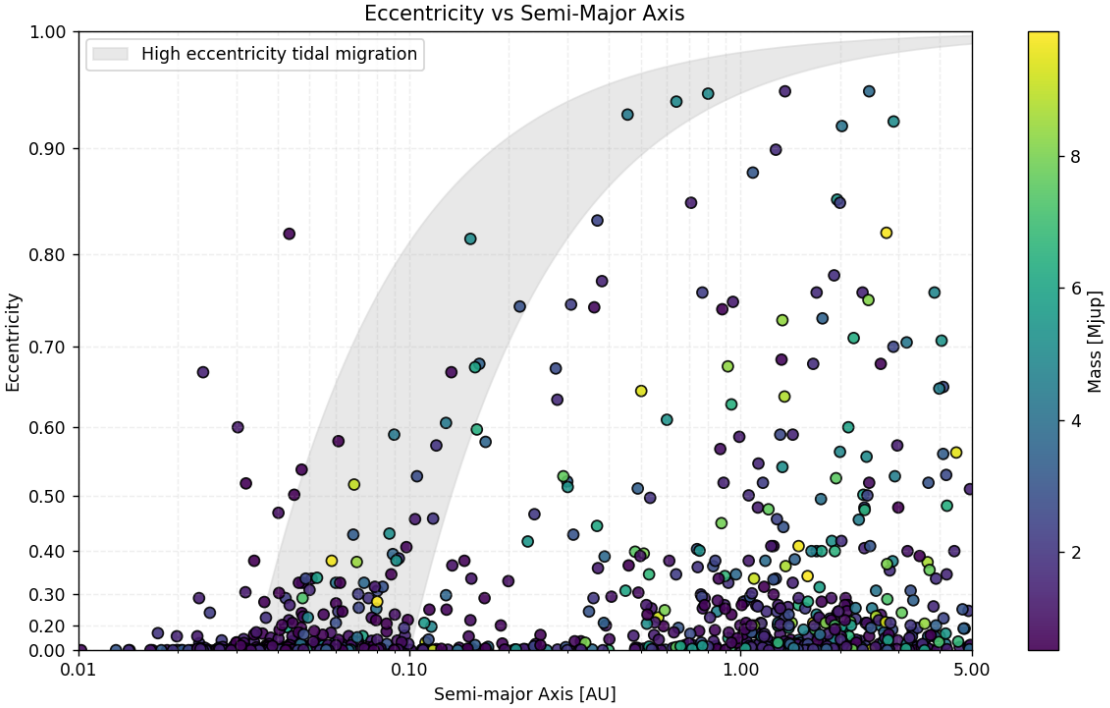

Figure 4.24: All observed planets with a semi-major axis of 0.01 AU $\leq a \leq$ 5 AU and a mass of 0.5 $M_{Jup} \leq m \leq$ 10 M_{Jup} according to the NASA Exoplanet Archive. The x-axis is in logarithmic scale, and the y-axis is scaled to e^2 to emphasize the highly eccentric planets.

5
Discussion

In this section I discuss my code and the results of this project. I also compare it to other scientific papers with a specific focus on why there was a lack of stable hot Jupiters from my results.

5.1 Code

A big deciding factor in this project is the code that was used to obtain the results. There was a lot of testing in the beginning to try to have the best possible code to use, specifically the tests that were done in section 4.1 to compare my code versus the code with Rebound. Except for the accuracy difference between my code and Rebound with the IAS15 integrator, another big reason as to why I used Rebound for the results was because of the time. While my code fully worked, albeit with a little worse accuracy, the time it took to run the same simulations as with Rebound was about 5-10 times longer. This is a major difference since the simulations already took a long time to run, up to 15 hours depending on the length of simulation and amount of varying parameters. Since I wanted to maximize the amount of parameters to vary and the length of the simulations, choosing to use Rebound because of the run time along with the accuracy difference was quite a clear choice. However, there are still some possible problems with using Rebound for this project worth discussing.

One possible issue is the oscillation of the eccentricity seen in figure 4.21. Specifically these oscillations are the worst in stable systems like the one seen in figure 4.21 where the oscillations in reality should be much smaller than this, but why this happens is not known.

Another problem is the choice of integrator to use for the project. While the accuracy of conservation of total energy and angular momentum was very good for IAS15 and better than the others in the tests, does that mean that I can trust it to be correct at all times? The fact of the oscillations in eccentricity does make it slightly less trustworthy. The IAS15 integrator also has the property that it automatically decreases the time step drastically in simulations where the two bodies get close to each other. This is of course good for the accuracy of the simulation, but it makes it impossible with my limited time and computational power to perform very long simulations over millions of years for more chaotic systems.

Probably the biggest reason, however, why my simulations were not able to produce stable hot Jupiters is the limited set of forces included in the default Rebound simulations. By default, Rebound integrates planetary orbits using Newtonian gravity, but additional physical effects such as general relativity or tidal dissipation are not included. During the course of this project, this limitation was not known. These effects, however, can be incorporated using the *REBOUNDx* extension, which provides modules for modeling the missing factors [38]. Integrating REBOUNDx into the simulation framework would be a valuable improvement for future work, especially when aiming for more realistic long-term evolution of hot Jupiters. The significance of these missing effects will be discussed in more in comparison to existing literature.

5.2 Output

The general consensus from all of my results are that the systems with a third body with high mass and high initial eccentricity has the highest likelihood of producing Jupiters with high eccentricity. A problem is that these systems with a high initial eccentricity are not expected to form since planets generally form with a very low eccentricity. This highly reduces the realistic aspect of these simulations. If we instead look at the simulations like figures 4.10 and 4.11 which are much more realistic with a third body initial eccentricity of 0, they are also capable of producing Jupiters on highly eccentric orbits. The percentage of systems that do this is however much lower for these initial conditions. Another problem with these more realistic systems are that the amount of collisions between planets increases drastically with time. This makes it very chaotic and hard to judge whether or not the planets that have not yet collided will do so later on or if they can become hot Jupiters.

One thing to mention though is that while many of my simulations ended with collisions between the two planets, this is not necessarily a failed system. Two planets colliding does not mean that the chance of creating a hot Jupiter goes to 0. It could be that they collide in such a way that the Jupiter is put in a highly eccentric orbit close to the Sun so that it could undergo HETM to become a hot Jupiter. This is however just a speculation and would require much more advanced simulations, which are outside the scope of this project.

5.3 Comparison to other literature

While the primary aim of this project was to simulate the formation of hot Jupiters via HETM, the simulations did not succeed in producing hot Jupiters in a stable and realistic way. This contrasts with several existing studies in the literature, which have either successfully produced hot Jupiters through numerical simulations or supported their formation pathways through observational evidence. To understand this discrepancy, I compare the methods, assumptions, and outcomes of my project with those of Beaugé & Nesvorný [35], Buchhave et al. [36], and Banerjee et al. [37].

One major difference concerns the parameter space and initial conditions. In this project, I varied three key parameters of the third planetary body: its mass m, initial semi-major axis a, and initial eccentricity e, while keeping Jupiter and the Sun fixed in all simulations. The setup was limited to a three-body system, and the third body's orbital inclination, argument of periapsis, and longitude of ascending node were set to zero, simplifying the system to two dimensions. In contrast, Beaugé & Nesvorný included systems with three or more planetary bodies interacting gravitationally, allowing for a richer set of dynamical behaviors including multiple rounds of scattering and resonances [35]. Their simulations varied not only masses and initial spacings but also included angular orbital elements and non-coplanar configurations. Similarly, Banerjee et al. based their analysis on observed planetary systems, which naturally reflect a wide diversity of architectures, often involving more than two planets [37]. Buchhave et al. focused on host star metallicity and its statistical correlation with giant planet formation, rather than dynamical simulations, but their conclusions are consistent with the presence of multiple gas giants in high-metallicity systems [36]. Overall, the limited number of bodies and restricted parameter space in my project, while useful for isolating specific behaviors, does not capture the full complexity of multi-planet systems likely to be responsible for forming hot Jupiters.

The accuracy of my setup when compared to real world scenarios is further questioned when considering other properties that were not accounted for in this project, such as host star metallicity. Buchhave et al. showed that hot Jupiter hosts tend to be metal-rich, supporting a formation environment conducive to multiple giant planets [36]. This, in turn, increases the likelihood of gravitational instabilities between planets that can drive inward migration. Banerjee et al. expanded on this by comparing hot, warm, and cold Jupiter systems and found that hot Jupiters often originate from systems with initially low eccentricities and relatively compact configurations [37]. In my case, some simulations began with highly excited systems that may not form naturally in such environments. Therefore, although the simulations produced chaotic dynamics, the specific conditions required for HETM to proceed in a physically realistic way were not always met.

Additionally, stability classification was handled differently. In my simulations, I judged outcomes primarily by tracking the final semi-major axis, eccentricity, and conservation of energy and angular momentum. In contrast, Beaugé & Nesvorný used more rigorous classification schemes that identified whether systems resulted in ejections, collisions, stable multiple-planet configurations, or successful hot Jupiter formation [35]. They also ran simulations over significantly longer timescales, often up to 10^8 years, compared to the more limited timescale I used, which was typically set by computational constraints.

Perhaps the most critical limitation of my project is the absence of non-Newtonian physical effects. Beaugé & Nesvorný clearly show that the formation of hot Jupiters through scattering and HETM requires both dynamical excitation and dissipative processes to shrink and circularize the orbit [35]. The forces that Beaugé & Nesvorný take into account except for Newtonian gravity between all bodies are tidal dissi-

pation, tidal precession, general relativity, and stellar oblateness, and without including these forces and corrections, even highly eccentric planets will not migrate inward [35]. This likely explains why, although some simulations did produce high-eccentricity orbits, none transitioned into true hot Jupiter configurations. It is also probably the single biggest reason why my simulations did not reproduce the results found in previous work.

Lastly, the use of observational data varies across studies. While I used the NASA Exoplanet Archive for some basic comparison, Banerjee et al. made direct use of observational data to constrain formation theories and derive statistical correlations [37]. Their approach integrates theory with real system properties, providing stronger observational grounding. Incorporating a similar data-driven approach into future simulation work could greatly enhance the realism and relevance of the results.

In summary, while this project provides insight into the dynamical behavior of three-body planetary systems under varying conditions, the lack of essential physical forces, limited simulation timescales, and suboptimally chosen initial conditions likely prevented the successful formation of stable hot Jupiters. The differences highlighted in these comparative studies offer a clear roadmap for improvements in future work.

6
Conclusion

The goal of this thesis was to explore the formation of hot Jupiters through the mechanism of high-eccentricity tidal migration (HETM), using numerical simulations to study the dynamical evolution of planetary systems. By modeling the gravitational interactions between the Sun, Jupiter, and a fictive third planet, the project aimed to assess whether specific initial configurations could trigger orbital migration that results in hot Jupiter formation. In a broader context, this work contributes to the ongoing effort to understand the diversity of planetary systems and the dynamical pathways that shape them.

A large set of simulations was conducted using a custom code as well as the Rebound N-body integration software. The project focused on a three-body, two-dimensional system, with variations applied to the third body's mass, semi-major axis, and eccentricity. My custom code and the code using Rebound was carefully validated against theoretical expectations of conservation of total energy and angular momentum of the individual systems. The accuracy check showed that the Rebound code with the IAS15 integrator was the most precise and was therefore used for the majority of the project.

One of the most consistent findings from the simulations was that a large portion of the tested initial conditions led to highly chaotic systems, often resulting in ejections or collisions. These outcomes were particularly common when the third body had high initial eccentricity or was placed too close to Jupiter. Many of the systems simulated ended up with a Jupiter with high eccentricity, and a decent portion of these had a low semi-major axis as well, which is required for it to undergo HETM. However, because of the unstable and chaotic nature of the systems, there is no guarantee that these would successfully undergo HETM and become hot Jupiters. In particular, no simulated planet achieved both high eccentricity and subsequent orbital shrinkage to the small semi-major axes characteristic of hot Jupiters. The most plausible explanation found for this outcome is the absence of non-Newtonian physical effects in the model. Tidal dissipation, tidal precession, general relativity, and stellar oblateness are known to play a critical role in converting eccentric orbits into circularized, close-in hot Jupiter orbits. Their omission is a likely—though not definitively proven—factor limiting the success of the simulations.

Comparisons to other work in the literature showed that studies which successfully formed hot Jupiters typically used more complete physical models and included more realistic planetary architectures, often with three or more planets. These studies also

used physical parameters informed by exoplanet observations, whereas this project initially explored broader and less constrained ranges. While this provided useful insight into general dynamical behaviors, future work would benefit from incorporating more astrophysically motivated setups.

The framework developed in this thesis lays the foundation for future studies into hot Jupiter formation via dynamical processes. A natural next step would be to extend the model using the `REBOUNDx` extension, which enables the inclusion of the additional forces that have to be accounted for. Another highly helpful improvement would be to somehow increase the computational power, allowing for longer simulations and more variations of parameters. Ultimately, this project demonstrates both the power and the limitations of gravitational simulations, and underscores the need for a more comprehensive treatment to accurately model the complex evolutionary history of planetary systems.

Bibliography

[1] M. Mayor and D. Queloz, "A Jupiter-mass companion to a solar-type star," , vol. 378, no. 6555, pp. 355–359, Nov. 1995.

[2] S. Ida and D. N. C. Lin, "Toward a Deterministic Model of Planetary Formation. II. The Formation and Retention of Gas Giant Planets around Stars with a Range of Metallicities," , vol. 616, no. 1, pp. 567–572, Nov. 2004.

[3] R. I. Dawson and J. A. Johnson, "Origins of Hot Jupiters," , vol. 56, pp. 175–221, Sep. 2018.

[4] J. B. Pollack, O. Hubickyj, P. Bodenheimer, J. J. Lissauer, M. Podolak, and Y. Greenzweig, "Formation of the giant planets by concurrent accretion of solids and gas," *Icarus*, vol. 124, no. 1, pp. 62–85, 1996. [Online]. Available: https://www.sciencedirect.com/science/article/pii/S0019103596901906

[5] S. T. S. Poon, R. P. Nelson, and G. A. L. Coleman, "In situ formation of hot Jupiters with companion super-Earths," , vol. 505, no. 2, pp. 2500–2516, Aug. 2021.

[6] C. Baruteau, A. Crida, S. J. Paardekooper, F. Masset, J. Guilet, B. Bitsch, R. Nelson, W. Kley, and J. Papaloizou, "Planet-Disk Interactions and Early Evolution of Planetary Systems," in *Protostars and Planets VI*, H. Beuther, R. S. Klessen, C. P. Dullemond, and T. Henning, Eds., Jan. 2014, pp. 667–689.

[7] A. J. Mustill, M. B. Davies, and A. Johansen, "The Destruction of Inner Planetary Systems during High-eccentricity Migration of Gas Giants," , vol. 808, no. 1, p. 14, Jul. 2015.

[8] H. Rein and contributors, "REBOUND documentation," https://rebound.readthedocs.io/en/latest/, 2025, accessed: 2025-05-16.

[9] J. J. Fortney, R. I. Dawson, and T. D. Komacek, "Hot Jupiters: Origins, Structure, Atmospheres," *Journal of Geophysical Research (Planets)*, vol. 126, no. 3, p. e06629, Mar. 2021.

[10] A. P. Showman, J. J. Fortney, Y. Lian, M. S. Marley, R. S. Freedman, H. A. Knutson, and D. Charbonneau, "Atmospheric Circulation of Hot Jupiters: Coupled Radiative-Dynamical General Circulation Model Simulations of HD 189733b and HD 209458b," , vol. 699, no. 1, pp. 564–584, Jul. 2009.

[11] NASA Exoplanet Science Institute, "Nasa exoplanet archive," https://exoplanetarchive.ipac.caltech.edu/, 2025, accessed: 2025-05-16.

[12] C. Hellier, D. R. Anderson, A. Collier Cameron, A. P. Doyle, A. Fumel, M. Gillon, E. Jehin, M. Lendl, P. F. L. Maxted, F. Pepe, D. Pollacco, D. Queloz, D. Ségransan, B. Smalley, A. M. S. Smith, J. Southworth, A. H. M. J. Triaud, S. Udry, and R. G. West, "Seven transiting hot Jupiters from WASP-South, Eu-

ler and TRAPPIST: WASP-47b, WASP-55b, WASP-61b, WASP-62b, WASP-63b, WASP-66b and WASP-67b," , vol. 426, no. 1, pp. 739–750, Oct. 2012.

[13] N. M. Batalha, J. F. Rowe, S. T. Bryson, T. Barclay, C. J. Burke, D. A. Caldwell, J. L. Christiansen, F. Mullally, S. E. Thompson, T. M. Brown, A. K. Dupree, D. C. Fabrycky, E. B. Ford, J. J. Fortney, R. L. Gilliland, H. Isaacson, D. W. Latham, G. W. Marcy, S. N. Quinn, D. Ragozzine, A. Shporer, W. J. Borucki, D. R. Ciardi, T. N. Gautier, III, M. R. Haas, J. M. Jenkins, D. G. Koch, J. J. Lissauer, W. Rapin, G. S. Basri, A. P. Boss, L. A. Buchhave, J. A. Carter, D. Charbonneau, J. Christensen-Dalsgaard, B. D. Clarke, W. D. Cochran, B.-O. Demory, J.-M. Desert, E. Devore, L. R. Doyle, G. A. Esquerdo, M. Everett, F. Fressin, J. C. Geary, F. R. Girouard, A. Gould, J. R. Hall, M. J. Holman, A. W. Howard, S. B. Howell, K. A. Ibrahim, K. Kinemuchi, H. Kjeldsen, T. C. Klaus, J. Li, P. W. Lucas, S. Meibom, R. L. Morris, A. Prša, E. Quintana, D. T. Sanderfer, D. Sasselov, S. E. Seader, J. C. Smith, J. H. Steffen, M. Still, M. C. Stumpe, J. C. Tarter, P. Tenenbaum, G. Torres, J. D. Twicken, K. Uddin, J. Van Cleve, L. Walkowicz, and W. F. Welsh, "Planetary Candidates Observed by Kepler. III. Analysis of the First 16 Months of Data," , vol. 204, no. 2, p. 24, Feb. 2013.

[14] J. P. Williams and L. A. Cieza, "Protoplanetary Disks and Their Evolution," , vol. 49, no. 1, pp. 67–117, Sep. 2011.

[15] A. N. Youdin and J. Goodman, "Streaming Instabilities in Protoplanetary Disks," , vol. 620, no. 1, pp. 459–469, Feb. 2005.

[16] A. P. Boss, "Giant planet formation by gravitational instability." *Science*, vol. 276, pp. 1836–1839, Jan. 1997.

[17] K. Batygin, P. H. Bodenheimer, and G. P. Laughlin, "In Situ Formation and Dynamical Evolution of Hot Jupiter Systems," , vol. 829, no. 2, p. 114, Oct. 2016.

[18] D. N. C. Lin, P. Bodenheimer, and D. C. Richardson, "Orbital migration of the planetary companion of 51 Pegasi to its present location," , vol. 380, no. 6575, pp. 606–607, Apr. 1996.

[19] Y. Wu and Y. Lithwick, "Secular Chaos and the Production of Hot Jupiters," , vol. 735, no. 2, p. 109, Jul. 2011.

[20] S. Naoz, "The Eccentric Kozai-Lidov Effect and Its Applications," , vol. 54, pp. 441–489, Sep. 2016.

[21] M. Nagasawa, S. Ida, and T. Bessho, "Formation of Hot Planets by a Combination of Planet Scattering, Tidal Circularization, and the Kozai Mechanism," , vol. 678, no. 1, pp. 498–508, May 2008.

[22] J. Dong, C. X. Huang, G. Zhou, R. I. Dawson, J. E. Rodriguez, J. D. Eastman, K. A. Collins, S. N. Quinn, A. Shporer, A. H. M. J. Triaud, S. Wang, T. Beatty, J. M. Jackson, K. I. Collins, L. Abe, O. Suarez, N. Crouzet, D. Mékarnia, G. Dransfield, E. L. N. Jensen, C. Stockdale, K. Barkaoui, A. Heitzmann, D. J. Wright, B. C. Addison, R. A. Wittenmyer, J. Okumura, B. P. Bowler, J. Horner, S. R. Kane, J. Kielkopf, H. Liu, P. Plavchan, M. W. Mengel, G. R. Ricker, R. Vanderspek, D. W. Latham, S. Seager, J. N. Winn, J. M. Jenkins, J. L. Christiansen, and M. Paegert, "TOI-3362b: A Proto Hot Jupiter Undergoing High-eccentricity Tidal Migration," , vol. 920, no. 1, p. L16, Oct. 2021.

[23] P. Hut, "Tidal evolution in close binary systems." , vol. 99, pp. 126–140, Jun. 1981.

[24] A. Bieryla, J. Dong, G. Zhou, J. D. Eastman, L. C. Mayorga, D. W. Latham, B. Carter, C. X. Huang, S. N. Quinn, K. A. Collins, L. Abe, Y. Beletsky, R. Brahm, K. D. Colón, Z. Essack, T. Guillot, T. Henning, M. J. Hobson, K. Horne, J. M. Jenkins, M. I. Jones, A. Jordán, D. Osip, G. R. Ricker, J. E. Rodriguez, J. Schulte, R. P. Schwarz, S. Seager, A. Shporer, O. Suarez, T.-G. Tan, E. B. Ting, A. Triaud, A. Vanderburg, J. N. Villaseñor, N. Vowell, C. N. Watkins, J. N. Winn, and C. Ziegler, "TOI-2005b: An Eccentric Warm Jupiter in Spin-orbit Alignment," , vol. 169, no. 5, p. 273, May 2025.

[25] H. D. Curtis, *Orbital Mechanics for Engineering Students (Third Edition)*, third edition ed., H. D. Curtis, Ed. Boston: Butterworth-Heinemann, 2014. [Online]. Available: https://www.sciencedirect.com/science/article/pii/B9780080977478000049

[26] A. V. Rao, "Orbital mechanics: An introduction," 08 2021.

[27] D. Kleppner and R. J. Kolenkow, *An Introduction to Mechanics.* McGraw Hill, 1973.

[28] M. Ezzelrgal, "Orbital mechanics," 06 2023.

[29] W. Press, S. Teukolsky, W. Vetterling, and B. Flannery, *Numerical Recipes: The Art of Scientific Computing (Third Edition).* Cambridge university press, 2007.

[30] H. Rein and S. F. Liu, "REBOUND: an open-source multi-purpose N-body code for collisional dynamics," , vol. 537, p. A128, Jan. 2012.

[31] H. Rein and D. Tamayo, "WHFAST: a fast and unbiased implementation of a symplectic Wisdom-Holman integrator for long-term gravitational simulations," , vol. 452, no. 1, pp. 376–388, Sep. 2015.

[32] H. Rein and D. S. Spiegel, "IAS15: a fast, adaptive, high-order integrator for gravitational dynamics, accurate to machine precision over a billion orbits," , vol. 446, no. 2, pp. 1424–1437, Jan. 2015.

[33] A. Ginsburg, B. M. Sipőcz, C. E. Brasseur, P. S. Cowperthwaite, M. W. Craig, C. Deil, J. Guillochon, G. Guzman, S. Liedtke, P. Lian Lim, K. E. Lockhart, M. Mommert, B. M. Morris, H. Norman, M. Parikh, M. V. Persson, T. P. Robitaille, J.-C. Segovia, L. P. Singer, E. J. Tollerud, M. de Val-Borro, I. Valtchanov, J. Woillez, Astroquery Collaboration, and a subset of astropy Collaboration, "astroquery: An Astronomical Web-querying Package in Python," , vol. 157, no. 3, p. 98, Mar. 2019.

[34] R. L. Akeson, X. Chen, D. Ciardi, M. Crane, J. Good, M. Harbut, E. Jackson, S. R. Kane, A. C. Laity, S. Leifer, M. Lynn, D. L. McElroy, M. Papin, P. Plavchan, S. V. Ramírez, R. Rey, K. von Braun, M. Wittman, M. Abajian, B. Ali, C. Beichman, A. Beekley, G. B. Berriman, S. Berukoff, G. Bryden, B. Chan, S. Groom, C. Lau, A. N. Payne, M. Regelson, M. Saucedo, M. Schmitz, J. Stauffer, P. Wyatt, and A. Zhang, "The NASA Exoplanet Archive: Data and Tools for Exoplanet Research," , vol. 125, no. 930, p. 989, Aug. 2013.

[35] C. Beaugé and D. Nesvorný, "Multiple-planet Scattering and the Origin of Hot Jupiters," , vol. 751, no. 2, p. 119, Jun. 2012.

[36] L. A. Buchhave, B. Bitsch, A. Johansen, D. W. Latham, M. Bizzarro, A. Bieryla, and D. M. Kipping, "Jupiter Analogs Orbit Stars with an Average Metallicity Close to That of the Sun," , vol. 856, no. 1, p. 37, Mar. 2018.

[37] B. Banerjee, M. Narang, P. Manoj, T. Henning, H. Tyagi, A. Surya, P. K. Nayak, and M. Tripathi, "Host-star Properties of Hot, Warm, and Cold Jupiters in the Solar Neighborhood from Gaia Data Release 3: Clues to Formation Pathways," , vol. 168, no. 1, p. 7, Jul. 2024.

[38] D. Tamayo, H. Rein, P. Shi, and D. M. Hernandez, "REBOUNDx: a library for adding conservative and dissipative forces to otherwise symplectic N-body integrations," , vol. 491, no. 2, pp. 2885–2901, Jan. 2020.

DEPARTMENT OF SOME SUBJECT OR TECHNOLOGY
CHALMERS UNIVERSITY OF TECHNOLOGY
Gothenburg, Sweden
www.chalmers.se

CHALMERS
UNIVERSITY OF TECHNOLOGY